HHS Public Access

Author manuscript

Nat Neurosci. Author manuscript; available in PMC 2024 December 19.

Published in final edited form as:

Nat Neurosci. 2024 January ; 27(1): 102–115. doi:10.1038/s41593-023-01482-6.

AgRP neurons encode circadian feeding time

Nilufer Sayar-Atasoy[1], **Iltan Aklan**[1], **Yavuz Yavuz**[1,2], **Connor Laule**[1], **Hyojin Kim**[1], **Jacob Rysted**[1], **Muhammed Ikbal Alp**[3], **Debbie Davis**[1], **Bayram Yilmaz**[2], **Deniz Atasoy**[1,4,5,✉]

[1]Department of Neuroscience and Pharmacology, University of Iowa, Iowa City, IA, USA.

[2]Department of Physiology, School of Medicine, Yeditepe University, Istanbul, Turkey.

[3]Department of Physiology, School of Medicine, Regenerative and Restorative Medical Research Center (REMER), Istanbul Medipol University, Istanbul, Turkey.

[4]Iowa Neuroscience Institute, University of Iowa, Iowa City, IA, USA.

[5]Fraternal Order of Eagles Diabetes Research Center (FOEDRC), Roy J. and Lucille A. Carver College of Medicine, University of Iowa, Iowa City, IA, USA.

Abstract

Food intake follows a predictable daily pattern and synchronizes metabolic rhythms. Neurons expressing agouti-related protein (AgRP) read out physiological energetic state and elicit feeding, but the regulation of these neurons across daily timescales is poorly understood. Using a combination of neuron dynamics measurements and timed optogenetic activation in mice, we show that daily AgRP-neuron activity was not fully consistent with existing models of homeostatic regulation. Instead of operating as a 'deprivation counter', AgRP-neuron activity primarily followed the circadian rest–activity cycle through a process that required an intact suprachiasmatic nucleus and synchronization by light. Imposing novel feeding patterns through time-restricted food access or periodic AgRP-neuron stimulation was sufficient to resynchronize the daily AgRP-neuron activity rhythm and drive anticipatory-like behavior through a process that required

✉ **Correspondence and requests for materials** should be addressed to Deniz Atasoy. deniz-atasoy@uiowa.edu.

Author contributions

N.S.-A. performed fiber photometry recording experiments and genotyping, prepared MATLAB and Arduino codes for data acquisition, analyzed the data and prepared the figures. I.A. and N.S.-A. performed surgeries. N.S-.A. and I.A. performed optoentrainment experiments. Y.Y., C.L. and I.A. performed electrophysiological recordings. H.K. and J.R. performed imaging. H.K., J.R., I.A. and N.S.-A. contributed to post hoc analysis. D.D. managed mouse breeding. M.I.A. and B.Y. contributed to behavioral setup instrumentation. D.A. and N.S.-A. conceived experiments and prepared the paper.

Competing interests

The authors declare no competing interests.

Reporting summary

Further information on research design is available in the Nature Portfolio Reporting Summary linked to this article.

Additional information

Extended data is available for this paper at https://doi.org/10.1038/s41593-023-01482-6.

Supplementary information The online version contains supplementary material available at https://doi.org/10.1038/s41593-023-01482-6.

Peer review information *Nature Neuroscience* thanks Zane Andrews and the other, anonymous, reviewer(s) for their contribution to the peer review of this work.

Code availability

MATLAB and Arduino scripts are available as Supplementary Codes 1–3.

DMH^{PDYN} neurons. These results indicate that AgRP neurons integrate time-of-day information of past feeding experience with current metabolic needs to predict circadian feeding time.

For most organisms, behavior and physiology vary in daily rhythms that are in synchrony with environmental cycles. As a dominant zeitgeber, feeding entrains extra-suprachiasmatic nucleus (SCN) clocks and drives metabolic and food anticipatory activity (FAA) rhythms[1]. The precise circuitry underlying feeding rhythms is poorly understood. Lesions in dorsomedial hypothalamus (DMH) impair FAA[2], and several gut hormones[3–6] and nutrient-activated reward pathways[7] have been implicated in synchronizing feeding time, but how these various components interact remains to be identified.

Hypothalamic 'hunger pathways' directly or indirectly interact with gut hormones, nutrients and reward circuits. Agouti-related protein (AgRP)-expressing neurons lie at the center of the hunger pathways and play a fundamental role in adapting to deprivation state physiology[8]. Although food-related cues transiently suppress their activity even before consumption[9], the current consensus assumes that the long-term regulation of AgRP-neuron activity is homeostatic, such that these neurons are activated by energy deficit and turned off by feeding. However, so far, studies have focused on relatively short time periods, and, thus, it remains unclear whether deprivation and satiety are the sole drivers of long-term AgRP-neuron dynamics.

Neonatal ablation of AgRP neurons and AgRP-neuron specific deletion of p75 or Crat have been shown to impair adaptation to restricted food access[10–13]. In addition, the clock gene *Bmal1* in AgRP neurons regulates transcriptional rhythms, and its deletion impairs leptin-induced transcriptional responses[14,15]. These studies point to a role for AgRP neurons in adapting to feeding schedules and in circadian regulation of their own transcriptional profile; however, whether and how circadian time interacts with homeostatic needs to modulate AgRP-neuron activity is unknown. It is also unknown how rhythmic cues, such as light or timed food access, influence chronic AgRP-neuron activity.

In this study, we addressed these questions by combining chronic in vivo activity recording with cell-type-specific manipulations. Our results reveal that time of day profoundly affects AgRP-neuron activity independently of ongoing feeding, and this requires SCN function in conditions of free food access and input from DMH prodynorphin (PDYN) neurons under scheduled food access.

Results

AgRP-neuron activity has a daily rhythm in vivo

To determine daily AgRP-neuron activity dynamics, we performed chronic Ca^{2+}-based in vivo fiber photometry recording from the arcuate nucleus (ARC) of *Agrp-ires-cre* mice transduced with *AAV-FLEX-CAG-GCaMP7s* or *AAV-CAG-FLEX-EGFP* (Fig. 1a,b and Extended Data Fig. 1a). Consistent with a previous report[16], we found that, with ad libitum (AL) food access, AgRP-neuron activity reached nadir just before the light onset (zeitgeber time 0 (ZT0)), after which it increased and peaked at ~ZT8. Dark onset (ZT12) induced a fast decline that further decreased during the dark phase (Fig. 1c,d,k and quantified

in Extended Data Fig. 1b). These oscillations were Ca^{2+} dependent because no apparent rhythmicity was observed in EGFP-expressing mice (Extended Data Fig. 1c).

Given that AgRP neurons are tuned to energy deficit and are rapidly suppressed by feeding[9,16,17], the drop at dark onset is likely mediated by ingestion, which might mask true AgRP-neuron activity rhythms. Consistent with this, daily AgRP-neuron activity was inversely correlated with feeding (Fig. 1e,f,i) and with locomotor activity (Extended Data Fig. 1d,e). Thus, to determine whether AgRP neurons have a food-independent activity rhythm, we removed food in the evening (ZT11) (Fig. 1g,h and Extended Data Fig. 1f) or morning (ZT22) (Extended Data Fig. 1g). In both cases, the drop in activity at dark onset was reversed, and relative AgRP-neuron activity increased soon after dark onset (quantified in Extended Data Fig. 1h), with the new peak significantly shifting to ~ZT18 (Fig. 1k). Notably, this fasted-state-induced increase at dark onset was not simply due to prolonged deprivation, because the rise was not gradual but, rather, occurred sharply after dark onset and because the activity returned to pre-dark phase levels by the next morning (Fig. 1h and Extended Data Fig. 1g). Consistent with higher AgRP activity during the night in the fasted state, the drop in Ca^{2+} signal was significantly larger if a cocktail of satiety hormones, known to silence overall AgRP-neuron activity[18], was delivered in the dark phase (ZT15) compared to the light phase (ZT3), even though both groups were fasted for the same duration (Extended Data Fig. 1i,j).

Given that AgRP neurons promote foraging and consummatory behaviors, we reasoned that the peaks in the food-independent activity pattern may reflect hours during which hunger drive is higher. Thus, we assessed whether fasted-state AgRP-neuron activity correlates with AL food intake in the same animals. Contrary to the fed state (Fig. 1i), fasted-state AgRP-neuron activity level correlated positively with the amount of the previous day's food intake at the same circadian hours (Fig. 1j and Extended Data Fig. 1k). Similarly, fasted-state AgRP-neuron activity correlated with locomotor activity (Extended Data Fig. 1l–o). These results suggest that time of day profoundly influences AgRP-neuron activity, such that the patterns in AL and fasted states are antiphase to each other (Fig. 1g,k). These findings also indicate an unprecedented uncoupling of long-term AgRP-neuron activity from homeostatic needs; instead, time of day appears to be the primary modulator.

AgRP-neuron activity rhythm is synchronized to light in AL food access

Chronic recordings suggested that light–dark (LD) transitions entail a major switch in daily AgRP-neuron activity, indicating that light may acutely and directly suppress AgRP-neuron activity to modulate feeding rhythm. Alternatively, light-dependent synchronization may occur indirectly over time, like other circadian activities.

To better understand the impact of light per se, we recorded AgRP-neuron activity along with feeding and locomotor activity rhythms under various light schedules. As expected, mice kept in constant darkness (DD) displayed normal locomotor activity and feeding rhythms, even after 9 d (Extended Data Fig. 2a,b). Consistently, in DD free-feeding mice, AgRP neurons maintained their daily activity pattern, with no significant decrease in circadian amplitude (Fig. 2a,b,g and quantified in Fig. 2i). Like in the normal LD cycle, food deprivation in DD increased AgRP-neuron activity at subjective dusk (circadian time

12 (CT12)), and activity remained relatively high until subjective dawn (CT0) (Fig. 2e,g and quantified in Fig. 2j). Conversely, under constant light (LL), the amplitude of AgRP-neuron activity rhythm was blunted in AL fed mice (Fig. 2c,d,h and quantified in Fig. 2i). This may not be due to a general behavioral arrhythmicity and resulting arrhythmic feeding (Extended Data Fig. 2c), because the same blunting was evident even in the absence of food (Fig. 2f,h,j).

Collectively, these findings suggest that the presence of a light cue is not required for day-to-day continuation of AgRP-neuron activity rhythm. Instead, the light dependence of AgRP-neuron activity and feeding rhythms might involve an entrainment-like process. Food-independent AgRP-neuron activity positively correlates with past circadian feeding pattern (Fig. 1j), which is tightly coupled to locomotor activity (Extended Data Fig. 2d–f). Therefore, overall circadian rest–activity rhythm may also shape daily AgRP activity rhythm, or both rhythms might be synchronized by the same source.

If light acutely controls AgRP-neuron activity, then a shift in the light phase would be expected to rapidly resynchronize its daily oscillations. Alternatively, the oscillations might be driven by a clock entrained to the LD cycle, in which case synchronization would appear slowly over several days. To gain further insight into synchronization to light, we exposed a set of mice that were previously under a 12-h light/12-h dark schedule to 8-h forward ‘jetlag’ phase shift by shortening the light phase. In the first day of 8-h forward shift, AgRP-neuron activity did not change significantly from the previous day with AL food access (Extended Data Fig. 2g,h). Instead, the activity slowly adapted to the new LD cycle over a week, along with locomotor activity and food intake (Fig. 2k–n). This adaptation paralleled food intake but lagged relative to the recovery of locomotor activity (Fig. 2q). We observed similar adaptation dynamics for food-independent AgRP-neuron activity, such that there was no significant change in the activity pattern on the first day of phase shift, but it slowly adapted to the new phase over a week (Fig. 2o,p and Extended Data Fig. 2i,j).

Taken together, these results further indicate that daily rhythms of food-dependent and food-independent AgRP-neuron activity are not directly or acutely responsive to light. Instead, AgRP-neuron activity slowly adapts to alterations in light cue over several days in a way that parallels entrainment of overall locomotor activity and feeding rhythms to circadian phase.

SCN is required for rhythmic AgRP-neuron activity in AL food access

Tuning of daily activities to light is coordinated by the SCN, which might provide instructions for AgRP-neuron synchronization with light. We performed bilateral lesions in the SCN via localized microinjection of taCasp3-expressing adeno-associated virus (AAV) (Fig. 3a,b). In line with earlier studies, SCN ablation flattened locomotor rest–activity and feeding rhythms (Fig. 3f,g and Supplementary Fig. 1a–e). Consistently, the amplitude of the AgRP-neuron activity rhythm was also blunted in free feeding (Fig. 3c,d,j and quantified in Fig. 3o) but not in the fasted state (Fig. 3i,j and quantified in Fig. 3p). However, when exposed to DD, any remaining oscillations were abolished (Fig. 3e,h,k,l,p and Supplementary Fig. 1f–h). These findings suggest that food-independent oscillations in circadian AgRP-neuron activity require either an intact SCN or light cues.

We next examined how the SCN communicates with AgRP neurons. Using optogenetic mapping[19], we did not detect any $SCN^{AVP} \rightarrow ARC^{NPY}$ or $SCN^{VIP} \rightarrow ARC^{NPY}$ connections (Supplementary Fig. 2). Although we cannot rule out the possibility that other SCN cell types might provide connections, it is likely that this interaction is mediated indirectly. We next examined corticosterone (cort), whose rhythmic variation is under SCN control and has been shown to remodel synaptic input, transcription and activity in AgRP neurons[20–23]. To test whether cort mediates daily AgRP-neuron activity rhythms, we impaired cort signaling specifically in AgRP neurons via cre-dependent overexpression of a cort-metabolizing enzyme using AAV-FLEX-11βHSD2-mCherry delivered together with AAV-CAG-FLEX-GCaMP7s into the ARC of *Agrp-ires-cre* mice[23,24] (Extended Data Fig. 3a). We found that, under AL food access, the amplitude of daily AgRP-neuron activity was not significantly different from control mice (Extended Data Fig. 3b–e and quantified in Fig. 3o). However, feeding rhythms were attenuated such that the large feeding bouts in early-dark onset were shifted toward the mid-dark phase, with larger meal sizes (Extended Data Fig. 3f–i). Furthermore, in fasted AgRP:HSD mice, timed activation of AgRP neurons at dark onset appeared to be blunted (Fig. 3m,n,p). This could be due to impairment in fasting-induced activation of AgRP neurons[23] or due to an overall blunting or shift in food-independent activity rhythms. Collectively, these results suggest that an intact SCN is required for AgRP-neuron activity rhythms and that cort signaling in AgRP neurons contributes to timely initiation of feeding at dark onset.

Synaptic input profile onto AgRP neurons varies with time of day

Given the limited impact of disrupted cort signaling on feeding rhythms, we next asked whether synaptic input contributes to AgRP-neuron activity rhythms. For this, we prepared acute hypothalamic slices from *Npy-gfp* mice at various timepoints throughout the day and recorded from GFP-labeled neurons in the ARC (Extended Data Fig. 4a). Previous work showed extensive overlap of ARC^{NPY} neurons with ARC^{AgRP} neurons (>98% of AgRP neurons also express NPY and >95% vice versa[25]). Consistent with this, in vivo daily activity patterns from ARC^{AgRP} (*Agrp-ires-cre*) neurons and ARC^{NPY} (*Npy-ires-flp*) neurons strongly correlated ($r = 0.85$, $P < 0.0001$). Henceforth, we will refer to ARC^{NPY} neurons as $ARC^{NPY/AgRP}$. Loose-seal recordings revealed that average ex vivo $ARC^{NPY/AgRP}$-neuron activity is highly dependent on the time of slice preparation, such that the firing rate was low and often involved silent neurons in slices prepared just before light onset, whereas firing rate was higher in slices prepared at noon (12:00) (Extended Data Fig. 4b,c). These results suggest that, in fresh hypothalamic slices, $ARC^{NPY/AgRP}$ neurons might maintain an activity pattern that parallels the in vivo rhythm.

To address whether changes in synaptic inputs drive AgRP-neuron activity rhythms, we isolated synaptic events with glutamate or GABA receptor blockade. Consistent with the slow rise in firing rate in the respective afternoon, spontaneous excitatory postsynaptic current (sEPSC) frequency increased from pre-light onset to afternoon. Conversely, spontaneous inhibitory postsynaptic current (sIPSC) frequency peaked just before light onset and sharply decreased by the afternoon (Extended Data Fig. 4d,e). Furthermore, under complete synaptic block, the late-afternoon peak in firing rate was blunted (Extended Data Fig. 4b,c). These results show that daily oscillations in synaptic input, such as the increase

in sEPSC/sIPSC ratio throughout the day, and likely combinations of other cell-autonomous and circulating factors, contribute to diurnal rise in AgRP-neuron activity.

To gain further insight into the role of synaptic (and extrasynaptic) input, we expressed fluorescent sensors for glutamate (iGluSnFR) or GABA (iGABASnFR) transmitters in AgRP neurons and chronically imaged their dynamics using fiber photometry (Extended Data Fig. 4f,n). We first tested how food access after fasting affects acute glutamate–GABA dynamics onto AgRP neurons. We found that glutamate signal rapidly and persistently drops after food access, whereas GABA drive briefly rises and then returns to baseline (Extended Data Fig. 4g–i,o–q). Next, we imaged daily variations in glutamatergic and GABAergic drive. Consistent with ex vivo recordings, under free food access iGluSnFR signal was significantly suppressed by dark onset and remained low until the next light onset. Surprisingly, a similar drop was observed in the absence of food, followed by a steady increase later in the dark phase (Extended Data Fig. 4j–m). This suggests that, in the fasted state, the initial phase of high AgRP-neuron activity at dark onset is unlikely to be mediated by increased excitatory input, whereas, later in the dark phase, marked increases in glutamate signal are consistent with elevated and sustained AgRP-neuron activity. By contrast, we did not observe a distinct circadian rhythm for iGABASnFR in free food access. However, in the absence of food, GABA signal showed a transient but significant decrease at dark onset, which then persistently increased throughout the dark phase (Extended Data Fig. 4r–u).

Taken together, our in vivo and ex vivo recordings suggest that daily variations in synaptic input profile may contribute to some features of daily AgRP-neuron activity but are unlikely to fully account for these rhythms.

Impaired upstream input dampens AgRP-neuron activity rhythm

To further dissect the role of network input, we ablated established upstream neurons. To assess excitatory synaptic drive, we examined input arriving from PVN^{TRH} neurons[26]. The PVN^{TRH} activity rhythm did not correlate with AgRP-neuron activity, and PVN^{TRH} neuron ablation did not significantly change feeding rhythms or daily $ARC^{NPY/AgRP}$-neuron activity patterns, suggesting that these neurons are dispensable for rhythmic appetite regulation (Extended Data Fig. 5).

We next addressed the contribution of inhibitory upstream input. The DMH is a downstream target of the SCN and integrates circadian and metabolic signals. DMH^{PDYN} neurons robustly inhibit AgRP neurons (Extended Data Fig. 6a–c)[27]. Thus, we reasoned that DMH^{PDYN} neurons may have an activity pattern opposite to AgRP neurons and that their input may contribute to daily AgRP-neuron activity. To address this possibility, we first tested whether DMH^{PDYN} neurons themselves have a daily activity rhythm using in vivo Ca^{2+} recording (Fig. 4a). In mice with AL food access, DMH^{PDYN} neurons had a complex activity pattern, with a sharp peak coinciding with dark onset, followed by a slow decline throughout the dark phase (Fig. 4b). Nevertheless, average daytime activity was lower than nighttime, which is opposite of AgRP-neuron activity (Extended Data Fig. 6d,e). Like AgRP-neuron dynamics, when food was removed, this pattern was mostly reversed. In the absence of food, the peak at dark onset persisted, but the subsequent drop was sharper

(Fig. 4c,d and Extended Data Fig. 6d). Relative DMH^{PDYN}- and $ARC^{NPY/AgRP}$-neuronal activities across the day in fasted mice were inversely correlated, supporting the possibility that DMH^{PDYN} neurons may contribute to daily AgRP-neuron activity rhythms (Fig. 4e).

To test this, we ablated DMH^{PDYN} neurons using caspase-expressing AAV. To validate ablation, we used unilateral AAV-FLEX-taCasp3 injection into the DMH region of *Pdyn-ires-cre* mice, and the contralateral side served as no-caspase control (Extended Data Fig. 6f). We then bilaterally ablated DMH^{PDYN} neurons in *Pdyn-ires-cre:Npy-ires-flp* mice and monitored $ARC^{NPY/AgRP}$-neuron activity as described above. After DMH^{PDYN}-neuron ablation, light-phase $ARC^{NPY/AgRP}$ activity was reduced, coinciding with increased food intake in late afternoon, and relative nighttime activity was increased; as a result, the overall amplitude of circadian activity in $ARC^{NPY/AgRP}$ neurons was blunted (Fig. 4f–k and Extended Data Fig. 6g). We also disrupted DMH^{PDYN} activity rhythm by chronic activation via targeted hM3D expression and chronically monitored activity of $ARC^{NPY/AgRP}$ using fiber photometry (Extended Data Fig. 6h). Chronic DMH^{PDYN}-neuron activation —by adding deschloroclozapine (DCZ) in drinking water under AL food access—resulted in a drop in daytime $ARC^{NPY/AgRP}$-neuron activity and reduced early dark-phase feeding but did not decrease overall daily amplitude (Extended Data Fig. 6i–r).

An altered $ARC^{NPY/AgRP}$ rhythm in mice with DMH^{PDYN} manipulations might be an indirect consequence of impaired feeding rhythms through an AgRP-neuron-independent circuit[28]. We, therefore, also recorded ARC^{NPY}-neuron activity in the absence of food. DMH^{PDYN} ablation flattened AgRP-neuron activity rhythms also in fasted mice (Fig. 4l–o). When DMH^{PDYN} neurons were chronically activated, the increased dark-phase $ARC^{NPY/AgRP}$-neuron activity was no longer observed, and the overall activity patterns were reversed (Extended Data Fig. 6s–u). This suggests that disinhibition from DMH^{PDYN} neurons might be required for the increased AgRP-neuron activity at dark onset in the fasted state.

Together, these results indicate that upstream input contributes to daily $ARC^{NPY/AgRP}$-neuron activity dynamics in a metabolic state-dependent manner, such that fasted-state rhythms are more susceptible to disrupted synaptic input, whereas, under AL food access, impaired upstream input attenuates feeding rhythm but does not abolish it.

Timed feeding overrides photic cues in shaping AgRP rhythms

Our recordings suggest that, when mice are fasted after free food access, AgRP-neuron activity mimics the past feeding pattern that is in sync with the overall rest–activity cycle. Namely, AgRP neurons are tuned to light, and this process requires an intact SCN. However, in the wild, most animals do not have free food access. Instead, strategies are often optimized to forage during a restricted time window. Therefore, we next asked how time-limited food access would influence the AgRP-neuron activity rhythm and its relation to the rest–activity cycle. For this, we first restricted feeding in the light phase (12 h, ZT0–ZT12), when mice are typically inactive and consume less. Light-cycle-only food access did not invert the daily rest–activity pattern, and these mice were still relatively more active at night; however, their locomotor activity pattern shifted such that relative activity in the early-dark phase and the late-dark phase was higher compared to AL feeding (Fig. 5a and Extended Data Fig. 7a). As expected, AgRP-neuron activity was lower in the light phase,

during which feeding occurred (Fig. 5b,c). Notably, although the inverse correlation between food intake and AgRP-neuron activity persisted, this was no longer the case for locomotor activity (Fig. 5d,e and Extended Data Fig. 7b,c). When food was not provided at light onset, AgRP-neuron activity rapidly climbed in the early-light phase and then steadily declined and reached nadir in the late-dark phase (Fig. 5f–h). This is in striking contrast to AgRP-neuron activity in mice fasted after free food access (Fig. 1h and Extended Data Fig. 1g). However, as in those mice, the daily patterns of AgRP-neuron activity and previous days' feeding, but not locomotor activity, remained correlated during light cycle restricted feeding (Fig. 5i,j). These findings suggest that, under a time-restricted feeding (TRF) regimen, mice adapt to the new feeding time, and daily AgRP-neuron activity uncouples from the circadian rest–activity cycle. When food is not provided during the anticipated TRF window, then AgRP-neuron activity increases and remains elevated until the end of the newly adapted feeding window.

The mice with 12 h of daytime food access showed weak but significant FAA before light onset. As reported previously[29], limiting food access even further (ZT3–ZT7) resulted in more prominent FAA (Extended Data Fig. 7f–h). To understand the temporal dynamics of AgRP-neuron activity adaptation to TRF access, we recorded daily activity on various days during a 4-h restricted feeding schedule. On the first day of TRF (ZT3–ZT7), activity rose and declined in the dark phase, which is effectively the same response as that seen in mice fasted after AL food access. Over the next several days in TRF, dark-phase AgRP-neuron activity was gradually flattened (Extended Data Fig. 7d,e). In line with earlier observations, at the time of food access, AgRP-neuron activity decreased, likely due to ongoing ingestion (Fig. 5k,l). The magnitude of food-mediated suppression was larger after a week in TRF compared to the first day (Fig. 5m). At the end of mealtime, activity slowly increased and plateaued by dark onset. There was no longer a significant positive or negative correlation between locomotor activity and AgRP-neuron activity under fed and fasted conditions, respectively (Extended Data Fig. 7i,j). Remarkably, if food was not presented at the anticipated time, AgRP-neuron activity rapidly surged to even higher levels (Fig. 5o). This activity surge was not present in the early days of the TRF regimen (Fig. 5n,p), likely because the AgRP neurons of these mice were still operating under the AL food access pattern (Fig. 1h). These findings further corroborate the observations from the 12-h daytime food restriction experiments, where AgRP-neuron activity patterns, both food dependent and food independent, shifted.

DMH^{PDYN} input is required for rhythmic AgRP-neuron activity

Results from mice under AL and scheduled feeding suggest that food-independent AgRP-neuron activity rises around the time of day that parallels the previous days' feeding time. This rise could play a role in keeping foraging and feeding activity in sync with earlier days' experience. We first confirmed that this rise depends only on food access time and not to a specific time of day. In mice entrained to feed at mid-dark phase (ZT18–ZT22), food omission resulted in a feeding-time surge in AgRP-neuron activity and locomotor activity similar to the mice TRF entrained to other times of day (Fig. 6a and Extended Data Fig. 8a–f).

To understand the underlying mechanisms, we performed several ablation studies. Cort levels increase near the entrained feeding time[30], and, given that cort can elevate AgRP-neuron activity[23], we tested whether a cort increase mediates the observed AgRP-neuron activation. As before, we impaired cort signaling specifically in AgRP neurons using virally overexpressed 11βHSD2 and exposed these mice to TRF while chronically monitoring in vivo AgRP-neuron activity. Impairing cort signaling specifically in AgRP neurons did not abolish AgRP-neuron activation at the entrained feeding time in the absence of food (Extended Data Fig. 8g).

We next tested whether the SCN plays role in timed AgRP activation in TRF. Although the SCN is not required for FAA in TRF, whether it contributes to AgRP-neuronal adaptation is unclear. Absence of AgRP synchronization to TRF in SCN-ablated mice would suggest that AgRP-independent mechanisms might compensate for timed feeding. To test this, we lesioned the SCN using a taCasp3-encoding AAV injection and exposed these mice to TRF. Unlike the marked effect on AL feeding rhythm (Fig. 3), SCN ablation had no effect on food-dependent or food-independent rhythms of AgRP-neuron activity in scheduled feeding (Extended Data Fig. 8h). To test whether the LD transition might be providing timing cues for AgRP activation, we kept SCN-ablated TRF mice in the dark for 14 d. Even in the absence of SCN and light cues, the TRF-entrained AgRP activity pattern persisted (Fig. 6b).

These findings suggest that feeding time activation of AgRP neurons after TRF entrainment might be mediated by a distinct mechanism than the one seen in mice fasted after AL food access. These results also support the possibility that, in SCN-ablated mice, the flattened AgRP-neuron activity rhythm might be secondary to arrhythmic feeding, because AgRP rhythms can be rescued with timed food access.

Previous reports suggested the DMH as a critical region for food entrainment[2,31]. Taken together with the known capacity of DMH neurons to modulate AgRP-neuron activity[27], we next explored this region. For this, we ablated DMH^{PDYN} neurons in *Pdyn-ires-cre:Npy-ires-flp* mice using cre-dependent AAV-taCasp3 injection and monitored $ARC^{NPY/AgRP}$-neuron activity. In DMH^{PDYN}-ablated TRF-entrained mice, timed $ARC^{NPY/AgRP}$-neuron activation was blunted (Fig. 6c). This was not due to the use of *Npy-ires-flp* line to probe $ARC^{NPY/AgRP}$-neuronal activity because the TRF-entrained control mice with the same genetic background and intact DMH^{PDYN} neurons had robust activation if food was not provided at the entrained time (Extended Data Fig. 8i). Additionally, none of the ablations abolished food-induced suppression of AgRP-neuron activity at the feeding time (Extended Data Fig. 8j–o). These findings suggest that DMH^{PDYN} neurons might be required for AgRP-neuronal adaptation to TRF. Consistently, when we monitored behavioral adaptation to TRF, we found that both FAA and timed feeding lagged significantly in DMH^{PDYN}-ablated mice (Fig. 6d–f). By contrast, mice with SCN or cort-signaling impairment adjusted their daily food intake faster than or similar to control groups, respectively[2,32,33]. Taken together, these findings show that, under scheduled feeding, the AgRP-neuron rhythm is uncoupled from the light phase and is synchronized to food access time through a process that requires DMH^{PDYN} input but not the SCN, cort signaling or light cue.

Impaired AgRP response to TRF in DMH^{PDYN}-ablated mice suggests that the DMH might provide time-sensitive input about food. If this is the case, then, in TRF-entrained mice, the activity of DMH^{PDYN} neurons should change depending on food. One possibility is that, in the absence of food, reduced DMH^{PDYN}-neuron activity at the anticipated feeding time may contribute to AgRP-neuronal disinhibition. To test this possibility, we imaged DMH^{PDYN}-neuronal activity in mice entrained with TRF (ZT3–ZT7) (Extended Data Fig. 9a). We then determined how omitting food at the entrained feeding time affects DMH^{PDYN}-neuron activity. DMH^{PDYN} neurons were indeed relatively more silent if food was not provided, as revealed by the difference between the daily signals of food-independent and food-dependent responses (Extended Data Fig. 9b–e). Notably, this relative reduction in activity coincided with the feeding window and the rise in $ARC^{NPY/AgRP}$ activity if food is omitted. Taken together, these results suggest that a reduction in DMH^{PDYN}-neuron activity may contribute to the timed activation of AgRP neurons at the feeding window.

Rhythmic AgRP-neuron activation partially mimics food entrainment

AgRP-neuron synchronization and behavioral adaptation to restricted feeding might be mediated by hunger-induced hormones, nutrients, other post-ingestive signals or a combination of these, rhythmically acting on central pathways. Because hunger causes a plethora of changes in the periphery and brain, identifying the relevant effectors poses a considerable challenge. AgRP neurons themselves play a key role in food deprivation response, and their artificial stimulation is sufficient to promote feeding and other physiological adaptations to hunger[17,34–36]. Thus, AgRP stimulation in fed mice can help avoid complexities associated with actual food deprivation and could be used to isolate the minimal signals sufficient for entraining. Accordingly, we designed an optogenetic entrainment protocol to periodically create a hunger-like state and feeding without actual food restriction. We expressed ChR2 in AgRP neurons of *Agrp-ires-cre* mice and repeatedly stimulated in respective midday (starting at ZT4), during which mice are normally inactive and eating is low. Stimulation continued for 4 weeks, with increasing stimulation time for 2 h, 4 h and 7 h per day, followed by intervening test days without food and stimulation (Fig. 7a–c). To test whether rhythmic AgRP activation is sufficient for entrainment, we monitored anticipatory locomotor activity before photoactivation start time for each stimulation day. We also monitored locomotor activity on no-food/no-stim test days (Fig. 7c).

As reported previously, AgRP activation caused feeding during photostimulation (Fig. 7b). Locomotor activity was also increased, consistent with increased wakefulness[37]. Significant increases in locomotor activity in the hours before photostimulation (ZT2–ZT4) emerged after the first week, suggesting the development of anticipatory-like behavior, even in AL conditions (Fig. 7d,e). Quantification of this activity revealed that its relative magnitude was smaller than those induced by actual TRF and was not visible in no-food/no-stim test day (Fig. 7f and Supplementary Fig. 3a). Notably, this increase was not due to an overall rise in locomotion because total daily activity did not change (Fig. 7g). Notably, too, at the end of stimulation days, we observed a sustained increase in daytime food intake that lasted for at least a week. This was not due to a general increase in feeding because total daily consumption was similar between stimulated and control groups (Fig. 7h and Supplementary Fig. 3b).

Because AgRP activation triggers feeding, the increased anticipatory-like locomotor activity may also require consumption. To test this possibility, we repeated, in a different set of mice, periodic stimulation in the absence of food. Periodic stimulation of AgRP-neuron activity alone was not sufficient to drive anticipatory-like activity (Supplementary Fig. 3c–g). Because food access rapidly reduces AgRP-neuron activity—a process that relieves hunger-induced negative valence—we reasoned that mice might be entrained to stimulation-end time when photostimulated in the absence of food. Indeed, locomotor activity increased in the period before stimulation cessation; however, this activity waned over days, which is inconsistent with anticipatory activity and likely due to AgRP stimulation-induced wakefulness itself (Supplementary Fig. 3h). Collectively, these results suggest that optogenetic entrainment via AgRP-neuron stimulation during inactive hours can promote anticipatory-like behavior through a process that requires food, and its magnitude is significantly smaller than actual TRF.

Under TRF, AgRP-neuron activity was higher in food access hours if food was not available (Fig. 5). To understand whether similar adaptations take place in optoentrained feeding, we performed loose-seal recordings from AgRP neurons of periodically stimulated mice. We observed that the firing rate of AgRP neurons was nearly twice that of control mice culled on respective mid-light phase, just before stimulation time (ZT4) (Fig. 7i,j). The increased activity was specific to the photostimulation period because no significant difference was observed if recording was performed from mice culled at the end of dark onset (ZT23).

In a separate set of experiments, we asked whether the increased feeding time activity in stimulated AgRP neurons was due to photoactivation and cell-autonomous mechanisms or if neighboring unstimulated AgRP neurons show a similar increase. We injected *Agrp-ires-cre* mice with *AAV-CAG-FLEX-ChR2-mCherry* on one side and *AAV-CAG-FLEX-GFP* on the contralateral side of the ARC (Fig. 7k). Loose-seal slice recordings at the end of 2 weeks of optoentrainment showed that average firing rate was increased similarly for both ChR2-expressing and $ChR2^{-}GFP^{+}$ AgRP neurons of the contralateral side around entrainment time, suggesting that AgRP photostimulation entrainment provides feedback signal to all AgRP neurons (Fig. 7l,m).

Collectively, these results reveal a timekeeping function upstream of AgRP neurons that is entrained by AgRP-driven feeding. Once entrained, this oscillator dictates rhythmic activity back to all AgRP neurons, including those that were not directly activated during optoentrainment.

Discussion

Current consensus on energy balance regulation predicts that hunger activates deprivation-sensitive AgRP neurons, which, in turn, stimulates feeding, and, once energy surfeit is achieved, these neurons go silent. Recent reports showing that AgRP-neuron activity suppression occurs by sensory food detection even before any calories are consumed[9,17] are inconsistent with such homeostatic regulation; nevertheless, long-term fluctuations are thought to report homeostatic needs. In the present study, using in vivo recording, we found that chronic dynamics of AgRP-neuron activity is not fully consistent with this view.

Three key observations showed that AgRP neurons do not simply function as a ‘deprivation counter’ as predicted by the homeostatic model. First, in fasted mice, AgRP-neuron activity did not increase gradually over food-deprived time, but, rather, it rose sharply at the anticipated feeding time (at dark phase or at food-entrained time). Second, more importantly, the activity did not stay high until energy surfeit was achieved, but, rather, it declined toward the end of the dark phase even when no calories were consumed; indeed, analysis of fasted-state AgRP-neuron activity throughout the day revealed a strong correlation with past feeding pattern (Fig. 1j). Third, the fluctuations in food-independent AgRP-neuron activity are not consistent with increased energy demand that could be caused by elevated locomotor activity. These observations suggest that, rather than simply reporting deprivation, AgRP-neuron activity follows a pattern that is consistent with past circadian feeding experience (Extended Data Fig. 10).

Although LD transitions were the major turning points for AgRP-neuron activity under free food access, the rhythm persisted in constant darkness, suggesting that a light cue is not acutely required. Additionally, phase shifting the light phase did not cause immediate resynchronization of AgRP-neuron activity and feeding rhythms, which slowly adapted instead (Fig. 2). These observations are more in line with light having an entraining role rather than being an on–off switch for AgRP neurons and feeding. How does light synchronize feeding rhythms? When food was freely available, feeding was tightly aligned with the active phase of the rest–activity cycle. One possibility is that light–SCN pathway-based signals actively synchronize AgRP-neuron activity—and, consequently, feeding—to the rest–activity cycle. Although we could not detect any direct effect of light on AgRP-neuron activity or any monosynaptic connection from SCN to AgRP neurons[38,39], there could be yet unidentified indirect routes mediating this interaction. Alternatively, synchronization of feeding to the rest–activity cycle might be a passive process secondary to increased wakefulness at dark. Because AgRP-neuron activity is synchronized to feeding over time, as seen in our TRF experiments, this would reinforce and effectively align AgRP-neuron activity with the rest–activity cycle. Our experiments with SCN ablation and constant light exposure cannot distinguish between these two possibilities. This is because, in both cases, AgRP-neuron activity rhythm was flattened along with overall behavioral rhythms[40], including feeding. Because feeding itself suppresses AgRP activity, desynchronized feeding would also desynchronize the daily AgRP rhythm. The observation that food-independent AgRP-neuron activity rhythms were also flattened in mice with a disrupted light–SCN pathway supports an active role for this pathway; however, we cannot rule out the possibility that this could be due to arrhythmic feeding before fasting.

Regardless of the specific mechanism, the end result is alignment of AgRP-neuron activity with the rest–activity rhythm. Notably, this alignment was unidirectional, and changes enforced on AgRP-neuron activity or feeding rhythm were not sufficient to reprogram daily rest– activity cycle. That is, under conditions of AgRP optostimulation or time-restricted feeding, there was indeed increased locomotor activity around the optostimulation and TRF window, respectively. However, this was not sufficient to resynchronize overall daily locomotor activity rhythms, likely due to the intact light–SCN pathway. Therefore, in optostimulated or TRF-entrained mice, AgRP-neuron activity was uncoupled from daily rhythms of locomotor activity.

An unexpected finding of this study is the rapid surge in AgRP-neuron activity at dark onset if food is not available. When mice are moved to TRF, the surge onset moved with food access time regardless of the light schedule. Thus, it is not the dark onset per se but the past circadian feeding time that drives this activity surge. Notably, even though AgRP-neuron stimulation increased locomotion in the presence of food, we do not think that the surge in AgRP-neuron activity drives FAA, because FAA precedes feeding time, whereas increased AgRP-neuron activity occurs soon after it if food is not found. However, the circuits driving FAA could be entrained by AgRP neurons, because their rhythmic optostimulation was sufficient to elicit an FAA-like behavior through a process that required consumption.

What drives this rapid rise in AgRP-neuron activity at the anticipated feeding time? Lesions to the DMH cause impairment in circadian feeding and cort rhythms[41,42]. Consistent with this, DMH^{PDYN}-neuron ablation flattened food-independent AgRP-neuron rhythm. Nevertheless, under AL food access, significant feeding and AgRP-neuron activity rhythm was sustained even after ablating DMH^{PDYN} or PVN^{TRH} neurons, suggesting that other factors might be involved in a metabolic state-dependent manner. Among likely alternatives, other synaptic inputs[26], astrocytes[43], internal clocks[14] and oscillating hormones could be involved. Indeed, selective disruption of cort signaling in AgRP neurons also attenuated feeding rhythm and flattened AgRP-neuron activity in the fasted state (Fig. 3n). This is in line with previous reports showing cort-mediated activation of AgRP neurons[23] via transcriptional changes[20,21] and synapse numbers on AgRP neurons[22]. Collectively, our results suggest that daily AgRP-neuron activity might be supported by redundant mechanisms in a nutritional-state-dependent manner, because no single manipulation selectively abolished its AL rhythm without disrupting overall rest–activity cycle.

Unlike the mice fasted after AL food access, the food-independent AgRP-neuron activity rhythm was insensitive to SCN ablation or cort signaling in TRF-entrained mice, supporting the notion that central and peripheral clocks decouple from the LD-tuned SCN[44,45] during restricted feeding. Although identifying the exact location of the food-entrained oscillator has been challenging[46], our results support a role for DMH^{PDYN} neurons. First, in line with previous studies[2,31,41,47], behavioral adaptation to TRF was attenuated in DMH^{PDYN}-ablated mice (Fig. 6d–f). Second, the food-independent AgRP-neuron activity surge at the scheduled feeding time was eliminated in DMH^{PDYN}-ablated mice (Fig. 6c). Third, consistent with previous work[2,32,33,48], DMH^{PDYN} neurons were responsive to scheduled feeding such that feeding onset transiently increased their activity, whereas lack of food at the anticipated time resulted in a sharp drop (Extended Data Fig. 9). These findings suggest that DMH^{PDYN} neurons might be a part of the food-entrained oscillator network and may act, in part, through its capacity to suppress AgRP-neuron activity.

How is this oscillator entrained in the first place? Given that AgRP-neuron activation alone is sufficient to drive many aspects of the food-deprived state, we reasoned that its rhythmic activity may instruct food-entrainable oscillators. Consistently, mimicking hunger state through rhythmic AgRP-neuron photostimulation induced anticipatory-like behavior (Fig. 7). However, AgRP-neuron optoentrainment did not fully recapitulate TRF, which might be due to persistent nocturnal feeding masking the full impact of photostimulation[49]. Nevertheless, consistent with previous studies[10–12,50], these experiments showed that

AgRP neurons are not only required for food entrainment but may also provide the key signals to trigger it. Among the possible downstream mediators for optoentrainment, photostimulation-induced ingestion and the resulting peripheral signals may play a key role[3,4]. Accordingly, omission of food during optostimulation abolished the anticipatory-like activity (Supplementary Fig. 3). Rhythmic AgRP-neuron activity may also affect downstream oscillator neurons or could cause the release of hormones with such potential[5,6]. Regardless of the specific mechanism, rhythmic feeding as a result of restricted food access or periodic activation of AgRP neurons caused a time-specific increase in AgRP-neuron activity itself in subsequent days, suggesting a reciprocal interaction with the putative oscillator.

Taken together, these observations support the idea that, rather than simply informing deprivation and following classical 'negative-feedback'-based homeostatic regulation, AgRP neurons may control energy balance through allostasis—that is, proactively adjusting their activity based on previous experience to fulfill future energy demands[51–53]. In this case, circadian time itself appears to act as a food-predictive cue. A priori modulation based on learned experience is also consistent with the observation that AgRP-neuron activity is suppressed by the sight of food even before any calories have been consumed[9,16,17].

Limitations of the study

Accessing ARC^{AgRP} neurons through *Npy* promoters (Npy-flp or Npy-gfp) has been used extensively in previous studies[26,54–57]. This is due to a high degree of co-localization between *Agrp* and *Npy* transcripts in the ARC (>98% of AgRP neurons co-express *Npy* transcript and ~95% of NPY neurons had *Agrp* transcript[25]). Consistent with this, we observed a strong correlation in the daily activity pattern of the two populations. However, we cannot completely rule out the possibility that a small amount of non-overlapping neurons may show different activity patterns under certain conditions.

Another limitation of this study is the possible damage of the ARC fiber placement to dorsal brain structures, especially the DMH, afferents and efferents. However, we think that such damage, if any, likely had limited impact because DMH^{PDYN} caspase-ablated mice had a significantly different ARC$^{NPY/AgRP}$-neuron activity pattern relative to control (Fig. 4i–o). Furthermore, DREADD-activated DMH^{PDYN} neurons rapidly suppressed ARC$^{AgRP/NPY}$-neuron activity (Extended Data Fig. 6b), suggesting that the former population is still functional and capable of influencing downstream neurons despite the fiber implant. For loss-of-function studies involving caspase ablation or HSD overexpression, we cannot rule out incomplete penetrance or the possibility that, during recovery from viral injection surgery, network compensatory changes may have taken place that can diminish the impact of ablations. We also did not monitor core body temperatures and cannot rule out the possible impact of hunger-induced torpor on chronic AgRP-neuron activity patterns. Finally, due to metabolic constrains of mice, our recordings of fasted-state rhythms were typically limited by approximately 1.5 cycles. Thus, it will be important to extend these findings using multi-day recordings without food in a more hunger-resilient model.

Conclusion

In summary, we showed that chronic variations in AgRP-neuron activity are not fully consistent with the homeostatic perspective. Instead, the schedule of previous feeding experience shapes chronic AgRP-neuron activity in subsequent days. Behaviorally, this would translate to increased hunger during adapted foraging hours and reduced hunger at other times[14]. That is, encoding circadian information about past feeding experiences into AgRP-neuron activity rhythms may promote foraging at similar hours on subsequent days to increase the chance of feeding and survival in an environment with rhythmic food availability. This may also prevent food seeking during non-optimal times of day when it might be futile or even dangerous. From a clinical perspective, because feeding powerfully entrains peripheral metabolic clocks, mis-timed feeding has detrimental consequences on metabolism by causing increased adiposity and decreased insulin sensitivity and longevity[58–60]. Our chronic recording and activation approach provides unprecedented insight into long-term regulators of AgRP-neuron activity and its role in entrainment. Future employment of these methods will likely provide further knowledge into downstream mediators.

Online content

Any methods, additional references, Nature Portfolio reporting summaries, source data, extended data, supplementary information, acknowledgements, peer review information; details of author contributions and competing interests; and statements of data and code availability are available at https://doi.org/10.1038/s41593-023-01482-6.

Methods

Animals

Mice used in this study were housed on 12-h LD, 24-h dark (DD) or 24-h light (LL) cycles at 20 −24 °C and 40–60% humidity, having AL access to standard chow food and water, unless going through restricted feeding. When required, animals were fasted for 18–36 h. For the TRF experiments, animals had access to chow between ZT0 and ZT12, ZT3 and ZT7 or ZT18 and ZT22, provided through automated FED3 feeders[61]. Mouse lines *Agrp-ires-cre* (Agrp$^{tm1(cre)Lowl}$, The Jackson Laboratory, 012899), *Npy-ires-flp* (The Jackson Laboratory, 030211), *Trh-ires-cre* (The Jackson Laboratory, 032468), *Pdyn-ires-cre* (The Jackson Laboratory, 027958), *Npy-gfp* (The Jackson Laboratory, 006417), *Avp-ires-cre* (The Jackson Laboratory, 023530) and *Vip-ires-cre* (The Jackson Laboratory, 010908) were back-crossed with C57BL/6 (The Jackson Laboratory, 000664) for maintenance. All studies were performed with 2–6-month-old male and female mice. Animal care and experimental procedures were approved by the University of Iowa Institutional Animal Care and Use Committee (IACUC, protocol no. 1082183) and YUDETAM (Istanbul, Turkey). Mice welfare and health checks were conducted in accordance with IACUC guidelines. Sentinel mice cages were periodically screened for pathogens. Mice that displayed unhealthy posture or more than 20% weight loss were removed from the study.

Stereotaxic surgeries

rAAV injections.—Stereotaxic surgeries were performed as described previously[62]. In brief, mice were anaesthetized with 1.5% isoflurane in the stereotaxic instrument (David Kopf Instruments). After disinfection, the scalp was incised to expose the skull, which was then drilled to obtain a small hole for injection. Then, 150–600 nl of virus was injected to each side intracranially using a pulled glass pipette (Drummond Scientific) with a 50-μm tip diameter. Viral injections were performed in the ARC (bregma: −1.20 mm, midline: ±0.25 mm, dorsal surface: −5.6 mm), the SCN (bregma: 0.35 mm, midline: ±0.25 mm, dorsal surface: −5.3 mm), the paraventricular nucleus (PVN) (bregma: −0.75 mm, midline: ±0.25 mm, dorsal surface: −5.0 mm) and the DMH (bregma: −1.15 mm, midline: ±0.35 mm, dorsal surface: −5.10 mm) for 50 nl min^{-1} by a micromanipulator (Narishige), allowing 10-min spread time for each injection. Scalp was stitched after removing the pipette and placing the optical fiber. At least 5–6 weeks were given for animal recovery and transgene expression before further experiments. Viruses used are listed below:

Company	Catalog number	Virus name
Addgene	104495	pGP-AAV-CAG-FLEX-jGCaMP7s-WPRE (AAV1)
Addgene	45580	pAAV-FLEX-taCasp3-TEVp (AAV5)
Addgene	105553	pENN-AAV-hSyn-Cre-WPRE.hGH (AAV5)
Addgene	44361-AAV2	pAAV-hSyn-DIO-hM3D(Gq)-mCherry (AAV2)
Viral Vector Facility Zurich	v521-DJ	ssAAV-DJ/2-hEF1a-dFRT-jGCaMP7s (rev)-dFRT-WPRE-hGHp(A)
Addgene	28306-AAV1	pAAV-FLEX-tdTomato (AAV1)
Addgene	106180	pAAV-hSynap-FLEX-SF-iGluSnFR. A184S (AAV5)
Addgene	112163	pAAV-hSyn-FLEX-iGABASnFR (AAV1)
Addgene	20298-AAV5	pAAV-EF1a-FLEX-hChR2(H134R)-EYFP-WPRE-HGHpA (AAV5)
Addgene	51502-AAV2	AAV pCAG-FLEX-EGFP-WPRE (AAV2)
Addgene	18916-AAV9	AAV-FLEX-rev-ChR2(H134R)-mCherry (AAV9)

Optical fiber placement.—Ferrule capped optical fiber (200 μm core diameter, numerical aperture (NA) = 0.50, Thorlabs, for in vivo optical stimulation; 200 μm or 400 μm core diameter, NA = 0.48, Thorlabs, for fiber photometry) was implanted above the ARC (bregma: −1.20 mm, midline: −0.25 mm, dorsal surface: −5.4 mm to −5.7 mm), above the PVN (bregma: −0.75 mm, midline: 0 mm, dorsal surface: 4.8–5.0 mm) or above the DMH (bregma: −1.15 mm, midline: ±0.35 mm, dorsal surface: −4.6 mm). Tip locations were positioned to be approximately 300 μm above the ARC or DMH for optostimulation fibers and ~100–200 μm for fiber photometry. Ferrule placements were performed after viral injection and fixed with dental cement.

In vivo fiber photometry recording and analysis.—After surgery recovery, animals were single housed in Plexiglass cages with free access to chow food (on the floor or through automated FED3 feeders) and cotton bedding and allowed 1–2 d of acclimatization to the cage. We then tethered the freely moving mice through their ferrule implants to the

fiberoptic cables (200-μm or 400-μm core, NA = 0.48, bundled fibers, Doric Lenses) using black ceramic mating sleeves (Thorlabs). Mice were allowed at least 3 d to acclimate to the tether before the fiber photometry experiments. In brief, fiber photometry was recorded at 3-Hz sampling rate using Doric FP Bundle Imager (Doric Lenses) and Doric Neuroscience Studio version 5.4.1.23. Light intensity for each wavelength at the end of the tip was set to be approximately 30–50 μW. For recordings from AgRP/NPY neurons, fasted subjects (24 h) that showed >10% $\Delta F/F$ signal decrease after food presentation were selected for further analysis (~60% of total injections). We recorded for 5 min or 10 min for every 30 min for multiple days[63]. Mice with problems with their feeding devices and/or timepoints where fibers were tangled or broken were removed from that day's analysis. At the end of recordings, mice were processed for post hoc histological evaluation. We eliminated animals where the virus or the fiber tip was off target.

For the analysis of the recorded data, we fit the isosbestic signal (405 nm) to the calcium-dependent signal (465 nm) using the linear least squares fit using a custom MATLAB script. Then, we calculated the $\Delta F/F$ as (465 nm − fitted 405 nm) / (fitted 405 nm) and averaged the 5 min (or 10 min) of data for each 30-min timepoint. To account for the inter-animal differences in signal intensities, we then calculated the z-scores from these values as $z = (F - F\mu) / F\sigma$, where F is the averaged $\Delta F/F$ value and $F\mu$ and $F\sigma$ are the mean and s.d. of the timepoints from the entire recording period.

For shorter recordings, at least 30 min of data were recorded before intraperitoneal injection of satiety cocktail (3 μg kg^{-1} CCK + 10 μg kg^{-1} amylin + 10 μg kg^{-1} PYY) or DCZ (Tocris, 0.5 μg kg^{-1}) (Extended Data Figs. 1j and 6b), and then the isosbestic signal was fit to the calcium-dependent signal, and $\Delta F/F$ values were calculated in the same way; however, z-scores were calculated using the mean and s.d. values of baseline data only as $z = (F - F\mu_{(Baseline)}) / F\sigma_{(Baseline)}$.

24-h food intake and actogram analysis.—Animals were single housed in home cages or custom-made Plexiglass cages with free access to chow food and cotton bedding and allowed 1–2 d of acclimatization to the cage and/or automated feeders. Food intake rhythms were collected using automated FED3 feeders (Open Ephys) and were converted to 30-min bins, unless stated otherwise, using FED3 Viz interface or custom MATLAB script.

For experiments with $DMH^{PDYN\text{-}hM3D}$ animals, assuming a mouse consumes 5 ml of water per day, we provided DCZ at 4 μg ml^{-1} concentration in water (prepared fresh daily) to chronically activate PDYN neurons, and change in food intake was followed using FED3 feeders.

Actograms were created using a custom setup with Arduino motion sensors (HC-SR501) and a custom script written in Arduino. Activity data were collected in seconds per 10 min, and each animal's data were normalized to its daily sum, unless stated otherwise.

Heat maps were created with Heatmapper (http://www.heatmapper.ca/expression/) using 30-min bins of food intake, actogram or GCaMP data, unless stated otherwise.

Optogenetic stimulation.—After recovery time, animals were single housed in custom-made Plexiglass cages and handled for being tethered to optical fibers for 2–3 d. After 5–7 d of baseline measurements, photostimulation was applied over the ARC using a 473-nm diode laser (10–15 mW from fiber tip, Doric Lenses). Pulse protocol used in this study was 10 Hz for 1 s repeated every 4 s, each pulse being 10 ms long. Food intake was recorded before tethering (at ZT0) and after untethering (at ZT8 or ZT10) of animals each day.

Electrophysiology.—P60–P90 mice were killed at various timepoints throughout the day, and recordings were performed within 2 h of culling. Brains were immersed in NMDG-HEPES aCSF cutting solution (in mM): 92 NMDG, 2.5 KCl, 1.25 NaH_2PO_4, 30 $NaHCO_3$, 20 HEPES, 25 glucose, 2 thiourea, 5 Na-ascorbate, 3 Na-pyruvate, 0.5 $CaCl_2 \cdot 2H_2O$ and 10 $MgSO_4 \cdot 7H_2O$. Brain tissue was kept in 95% O_2/5% CO_2 aerated ice-cold cutting solution, and 300-μm-thick fresh slices containing the ARC were obtained with a vibratome and transferred to 95% O_2/5% CO_2 aerated and HEPES-containing aCSF incubation solution containing (in mM): 92 NaCl, 2.5 KCl, 1.25 NaH_2PO_4, 30 $NaHCO_3$, 20 HEPES, 25 glucose, 2 thiourea, 5 Na-ascorbate, 3 Na-pyruvate, 2 $CaCl_2 \cdot 2H_2O$ and 2 $MgSO_4 \cdot 7H_2O$. The sections were incubated in this solution for at least 30 min and placed in the recording chamber that has the recording aCSF (in mM): 124 NaCl, 2.5 KCl, 1.25 NaH_2PO_4, 24 $NaHCO_3$, 12.5 glucose, 5 HEPES, 2 $CaCl_2 \cdot 2H_2O$ and 2 $MgSO_4 \cdot 7H_2O$. Loose-seal and whole-cell patch-clamp recordings were performed on AgRP/NPY neurons using electrodes with 4–5 MΩ tip resistances. For loose-seal recordings, aCSF was used as the pipette solution. For recordings requiring synaptic blockers, CNQX (10 μM) + AP5 (50 μM) were added to block excitatory transmission, and PTX (50 μM) was added to block $GABA_A$ receptors. For whole-cell recordings, pipette solution contained (in mM): 125 CsCl, 5 NaCl, 10 HEPES, 0.6 EGTA, 4 Mg-ATP, 0.3 Na_2GTP, 10 lidocaine N-ethyl bromide (QX-314), pH 7.35, and 290 mOsm. The holding potential was set to −60 mV. For SCN → ARC connectivity experiments (Supplementary Fig. 2), no synaptic blockers were added to the medium. In whole-cell configuration, 3–5 sweeps were collected while photostimulating $SCN^{AVP:ChR2}$ or $SCN^{VIP:ChR2}$ axons with pulses at 10 Hz. For connectivity using loose seal, 90-s recordings were acquired, and stimulation was given between 30 s and 60 s. MultiClamp 700B Amplifier (Molecular Devices) and Axon pCLAMP 11 software (Molecular Devices) were used to obtain and analyze data.

Histology and imaging.—Upon completion of experiments, to verify viral expression and ferrule locations, animals were anesthetized and transcardially perfused with PBS, followed by 4% paraformaldehyde (PFA). Extracted brains were further fixed in 4% PFA for 4 h and preserved in 30% sucrose solution. Then, using a vibrotome (Campden Instruments), 100-μm-thick coronal sections were obtained and were either directly mounted using FluoroShield with DAPI (Sigma-Aldrich) or further processed with immunostaining. Mice with weak or no fiber photometry signal had poor infection or mis-targeted fiber tip location. For DMH^{PDYN} ablation experiments, *AAV-FLEX-taCasp3* was mixed with AAV-hSyn-tdTom (1:2 volume ratio) to mark the site of viral injection. A total of 150 nl per side was injected. To verify successful ablation of the SCN, slices containing the SCN region were labeled with primary antibody for vasointestinal peptide (VIP, ImmunoStar, 20077,

1:7,500) and secondary antibody Alexa Fluor 647 goat anti-rabbit (A-21244, 1:500, Thermo Fisher Scientific). After mounting, we imaged sections on an Olympus slide scanner.

Statistical analysis.—The number of mice in each cohort was estimated based on pilot experiments and previously published work[34,62–64]. Data distribution was assumed to be normal; however, this was not formally tested. Outlier tests were not performed. Where possible, experiments were repeated with an independent cohort, and results were combined for final analysis. Mice were randomly assigned to groups. Initial planning of experimental groups was not blinded, but, where possible, investigators were blinded for the experiment and data analysis.

Differences between two groups were tested with paired and unpaired two-sided *t*-tests. Multiple group statistical comparisons were made by one-way analysis of variance (ANOVA) or two-way repeated-measures ANOVA, and corrected *P* values and Pearson *r* and *P* values were calculated using GraphPad Prism 8.1 (GraphPad Software). Rayleigh test for non-uniformity of circular data and circular ANOVA to compare circular data were calculated using the Circular Statistics Toolbox in MATLAB[65]. Circadian rhythmicity was calculated in R, using JTK_CYCLE[66]. '*n*' represents mice or neuron numbers as indicated for each experiment. $P < 0.05$ was considered to be statistically significant. The representative images and recording traces provided in the figures were similar for the *n* number of repetitions provided in relevant sections.

Extended Data

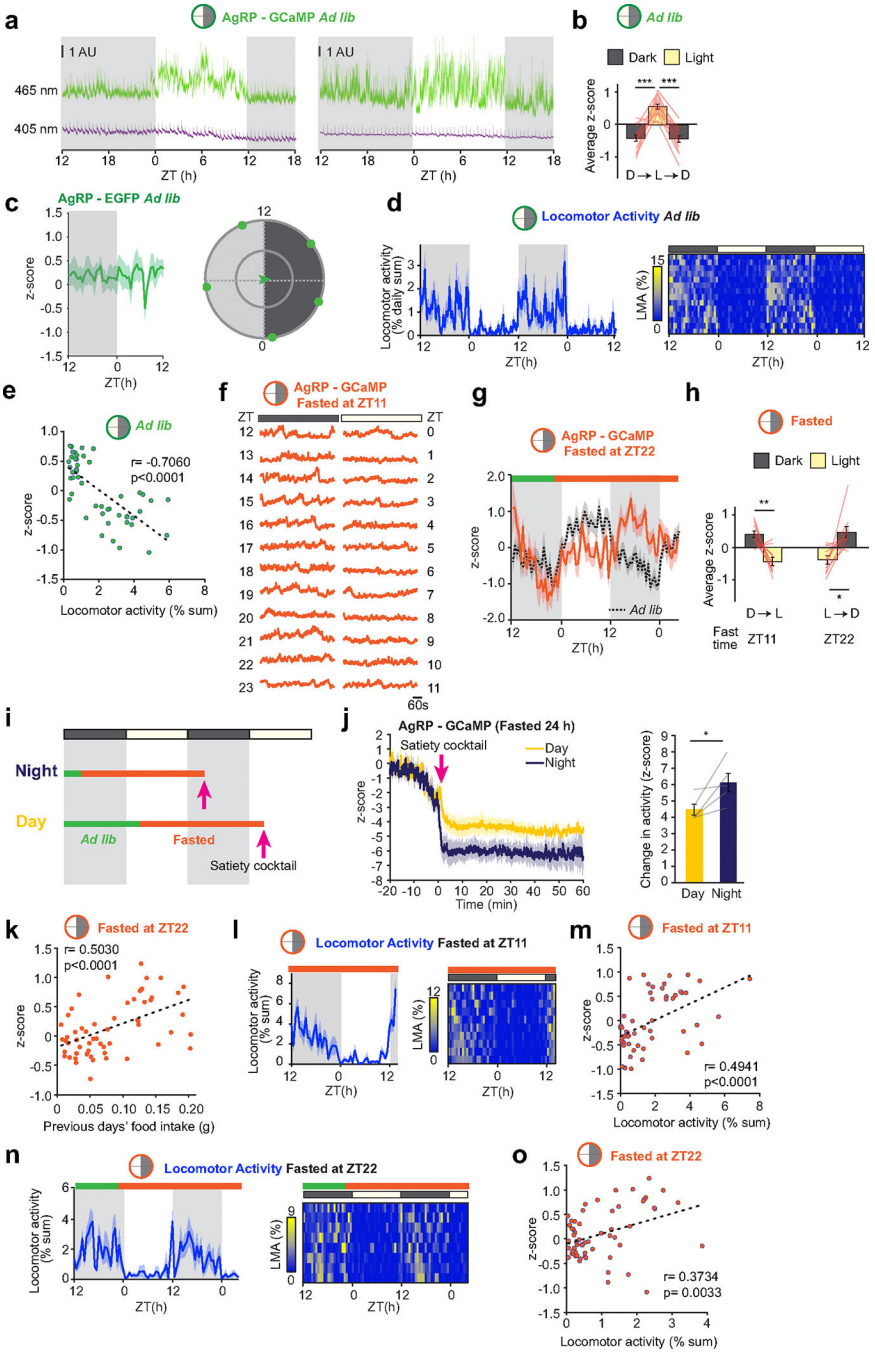

Extended Data Fig. 1 |. AgRP-neuron activity shifts to anti-phase in the absence of food.

a. Representative concatenated raw 465 and 405 traces recorded 5 minutes every 30 minutes from AgRP-neurons under *AL* conditions. Dark shade: dark phase, no shade: light phase. **b**. Average AgRP activity in dark and light phases (n = 14 mice, two-tailed paired t-test, ***p < 0.0001). **c**. Left: Averaged daily AgRP GFP activity (n = 5 mice). Right: Rayleigh-plot of AgRP:GFP rhythm in *AL* fed mice, mean peak: ZT17.7, not significant. **d**. Daily

locomotor activity (normalized to total daily activity of each animal) in LD (left panel) and its heatmap showing each animal's data (right panel). n = 14 mice. **e**. Two-tailed Pearson correlation between AgRP-neuron activity and locomotor activity across same circadian time points under *AL* conditions. **f**. Representative hourly AgRP GCaMP7s traces (z-score) recorded from mice fasted at ZT11, by acquiring for 10 min at every 30 mins in LD (12 h light:12 h dark). Yellow bar: Light phase, dark gray bar: dark phase. **g**. Averaged AgRP GCaMP7s rhythms recorded from mice fasted at ZT22 (n = 8 mice). Dashed line is from *AL*. **h**. Change in AgRP GCaMP activity in dark and light phases in mice fasted at ZT11 or at ZT22 (two-tailed paired t-test, n = 10 animals, **p = 0.00304, *p = 0.0148) **i**. Scheme describing the protocol in j. **j**. Left: AgRP GCaMP activity recorded from 24 h fasted mice that were injected satiety-hormone cocktail during day (ZT3), or night (ZT15). Right: Quantification of activity drop by satiety hormones. **k**. Two-tailed Pearson correlation between AgRP-neuron activity from mice fasted at ZT22 and previous days' average food intake across the same circadian timepoints. **l**. Locomotor activity recorded from mice that were fasted at ZT11 (left panel) and heatmap showing each animal's data (right panel). n = 10 mice. **m**. Two-tailed Pearson correlation between AgRP-neuron activity (z-score) and locomotor activity across same circadian time points under fasted conditions (fasting started at ZT11). **n,o**. Same with l,m, but mice were fasted at ZT22. Data are presented as mean ± SEM. For exact P-values and statistics, see Extended Data Fig. 1 Source Data.

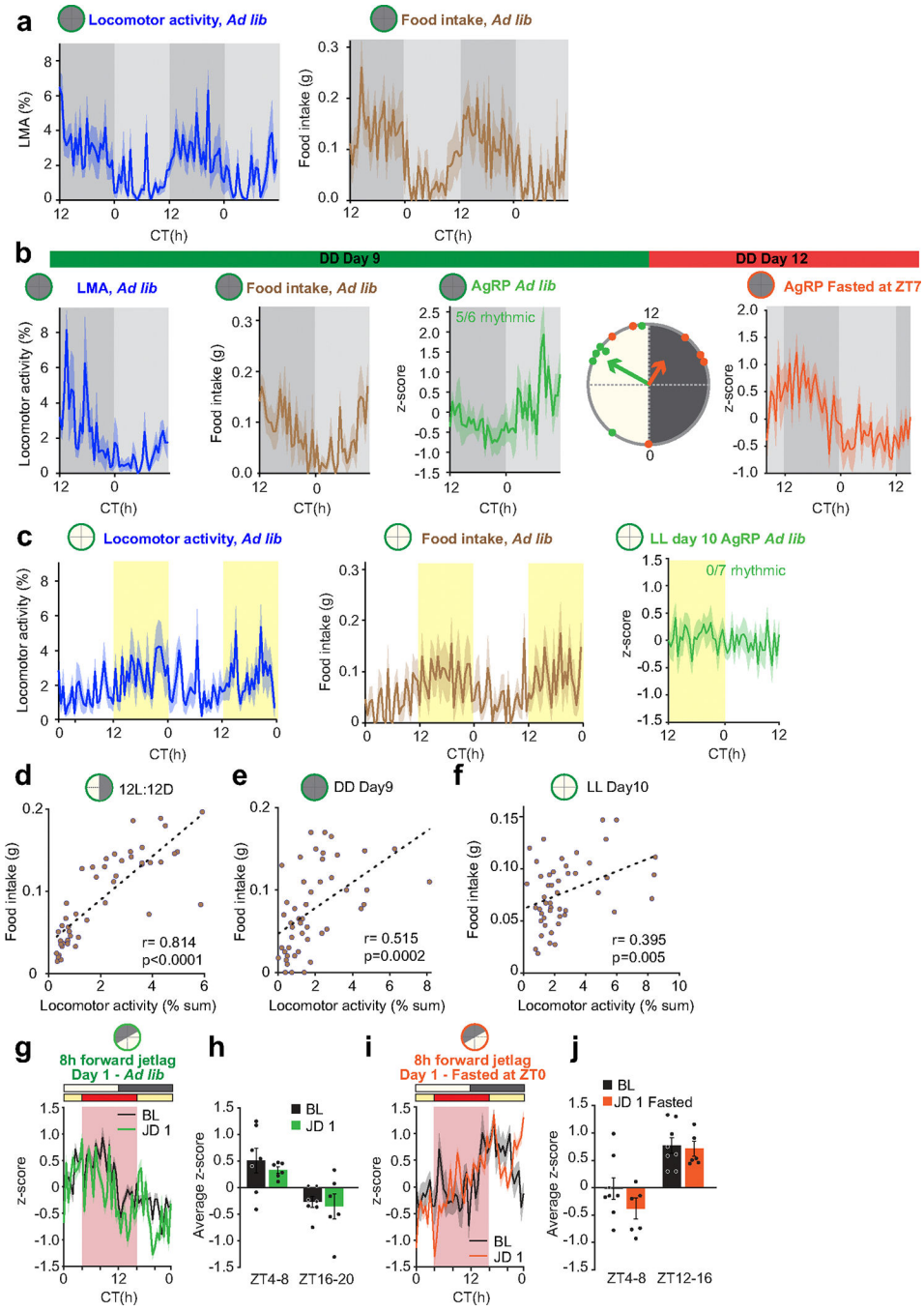

Extended Data Fig. 2 |. Effect of light schedule on AgRP-neuron rhythms.

a. Average locomotor activity (left) and food intake (right) rhythms in the first days of constant dark (DD, left, 6 mice). **b**. Average locomotor activity, food intake, AgRP GCaMP rhythms (5/6 mice were still rhythmic) under *AL* conditions, Rayleigh-plots (*ad lib* and fasted phases differ significantly, p = 0.0329, circular one-way ANOVA), and AgRP activity under fasted conditions, respectively, in later days of DD light setting. **c**. Average locomotor activity (left) and food intake (middle) rhythms in the first days of constant light (LL, 8 mice) and AgRP GCaMP activity on 10th day of LL setting (right). 0/7 animals were

rhythmic. **d-f**. Two-tailed Pearson correlation between average food intake and locomotor activity across same circadian time points under 12 h Light :12 h Dark (d), DD day 9 (e), and LL day 10 (f). **g,h**. Average AgRP-neuron activity on baseline day (BL, 7 mice) overlaid with the first jetlag day (JD-1, 6 mice) (g) and quantification of post light phase shift mid-dark phase and mid-light phase average AgRP activities (h) in *AL* fed mice. **i,j**. Same as (g,h) except no food was provided (8 BL, 6 JD-1 mice). Data are presented as mean ± SEM. For exact P-values and statistics, see Extended Data Fig. 2 Source Data.

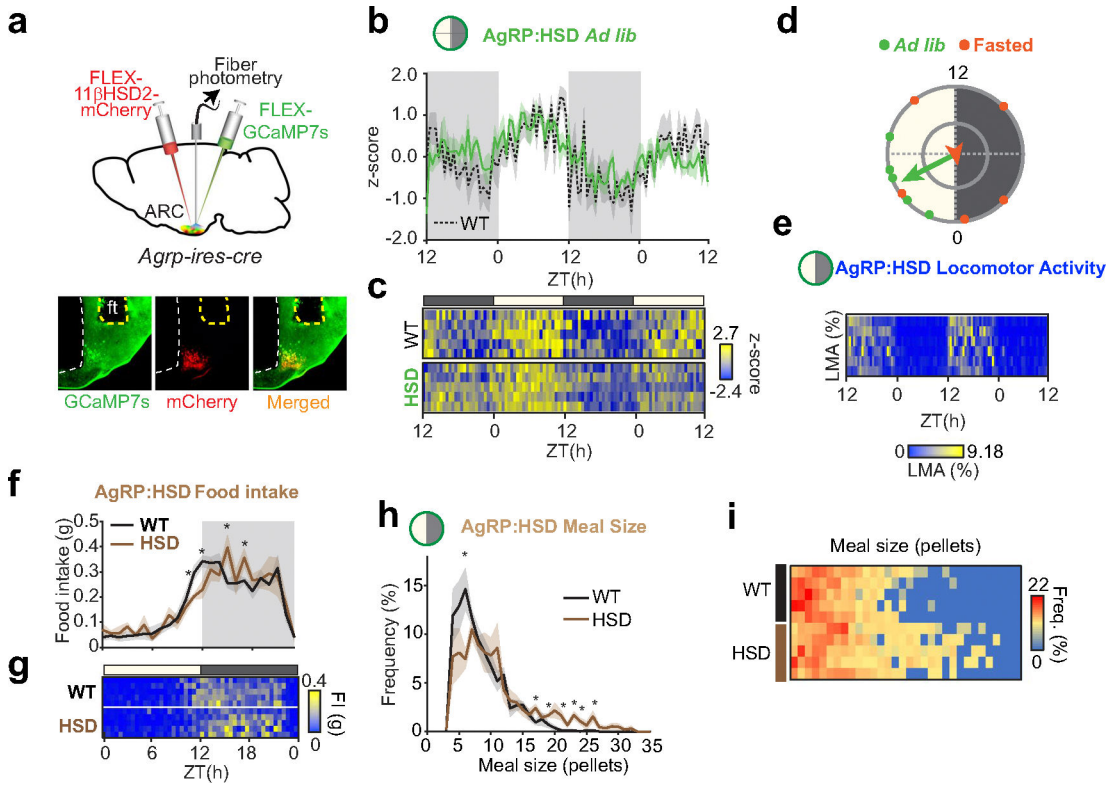

Extended Data Fig. 3 |. AgRP-neuron specific disruption of cort signaling alters feeding time and meal pattern.

a. Schematic of *in vivo* fiber photometry recording of AgRP calcium activity in AgRP specific 11βHSD2 expressing (HSD) mice, and representative images showing GCaMP and 11βHSD2 expression in AgRP cells. **b,c**. Average (b) and individual (heatmap, c) AgRP GCaMP7s activity rhythms recorded from AgRP:HSD mice compared to WT mice in free feeding. **d**. Rayleigh-plots of AgRP rhythms in HSD animals under *AL* (mean peak times at ZT4.9, Rayleigh p = 0.0113, Rayleigh test for non-uniformity of circular data) and fasted (mean peak time at ZT23.33, not significant, Rayleigh test for non-uniformity of circular data) conditions. Phases do not differ significantly (one-way circular ANOVA, n = 5 mice each). **e**. Heatmap showing individual AL locomotor activity in AgRP:HSD mice. **f,g**. Average (f) and individual (heatmaps, g) daily food intake in AgRP:HSD mice compared to WT mice. Average of 6 days has been shown, n = 5 mice each (two-tailed unpaired t-test, ZT11 *p < 0.05). **h,i**. Averaged (h) and individual (i) meal size frequencies in wild type and HSD mice (two-tailed unpaired t-test, 6 pellets *p < 0.05). Data are presented as mean ± SEM. For exact P-values, and statistics, see Extended Data Fig. 3 Source Data.

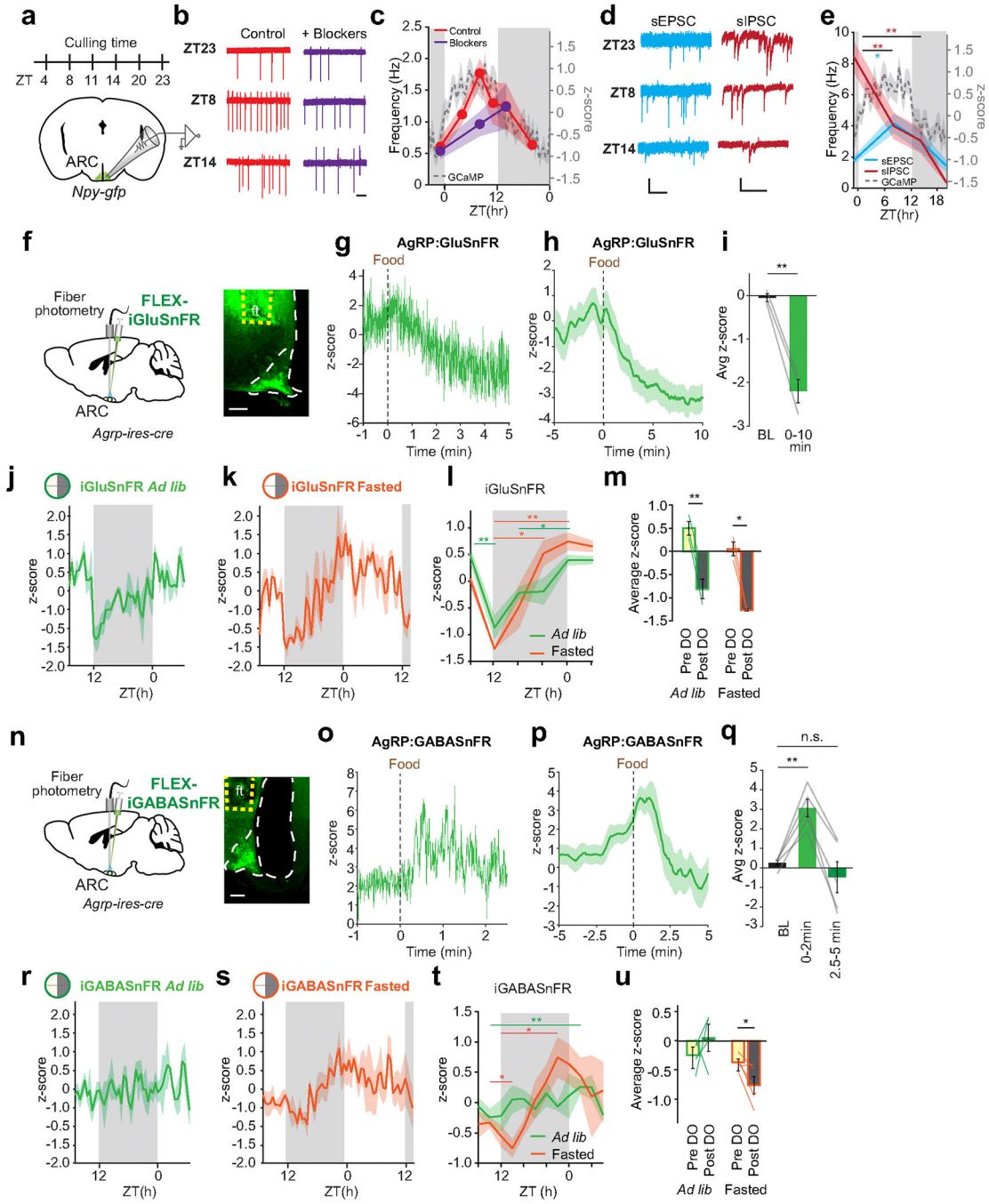

Extended Data Fig. 4 |. Circadian variations of synaptic input contribute to AgRP-neuron activity rhythms.

a. Schematic of *ex-vivo* recording from GFP labeled ARC^{NPY} neurons in *Npy-gfp* mice and culling times. **b,c**. Representative loose-seal traces (b, scale: 1 s) and average ARC^{NPY} neuron activity (c) overlaid with average *in vivo* AgRP:GCaMP7s trace. n = 39–82 neurons for control, and n = 8–19 neurons for data with synaptic blockers. **d,e**. Representative whole-cell recordings from ARC^{NPY} neurons showing synaptic events (d) and average (e) spontaneous IPSC and EPSC frequency across day overlaid with average *in vivo*

AgRP:GCaMP7s activity. n = 8–17 neurons for sEPSC, and n = 6–22 neurons for sIPSC, two-tailed, unpaired t-test, *p < 0.05, **p < 0.01. Scale: 2 s, 20 pA (sEPSC), 50 pA (sIPSC) **f**. Schematic of *in vivo* fiber photometry recording of glutamate dynamics on AgRP-neurons and representative image showing AgRP cells expressing iGluSnFR, and the placement of the fiber in the ARC (Scale 100 μm). **g-i**. Representative AgRP- iGluSnFR raw trace (g) and averaged signal (h) recorded during access to food in fasted mice and quantification of changes in iGluSnFR signal in the first minutes of food access (two-tailed paired t-test, p = 0.008, n = 3 mice, i). **j-l**. Summary of changes in glutamate levels on AgRP-neurons over 24 h in *AL* (average of 3 animals, 3 days, j) and fasted (k) animals, and overlay of two rhythms in averaged in 4 h bins (l, two-tailed paired t-test, *p < 0.05, **p < 0.01). **m**. Comparison of pre-dark onset (ZT8-ZT12) and dark onset (ZT12-ZT16) levels of glutamate on AgRP-neurons in *AL* and fasted animals (two-tailed paired t-test, **p = 0.0024, *p = 0.013, n = 3 mice). **n-u**. Same as f-m, except iGABASnFR was examined (**p = 0.0025, q; **p = 0.0076, *p < 0.05, t; *p = 0.029, u, n = 4 *ad lib*, n = 5 fasted). Data are presented as mean ± SEM. For exact P-values, number of subjects/neurons, and statistics, see Extended Data Fig. 4 Source Data.

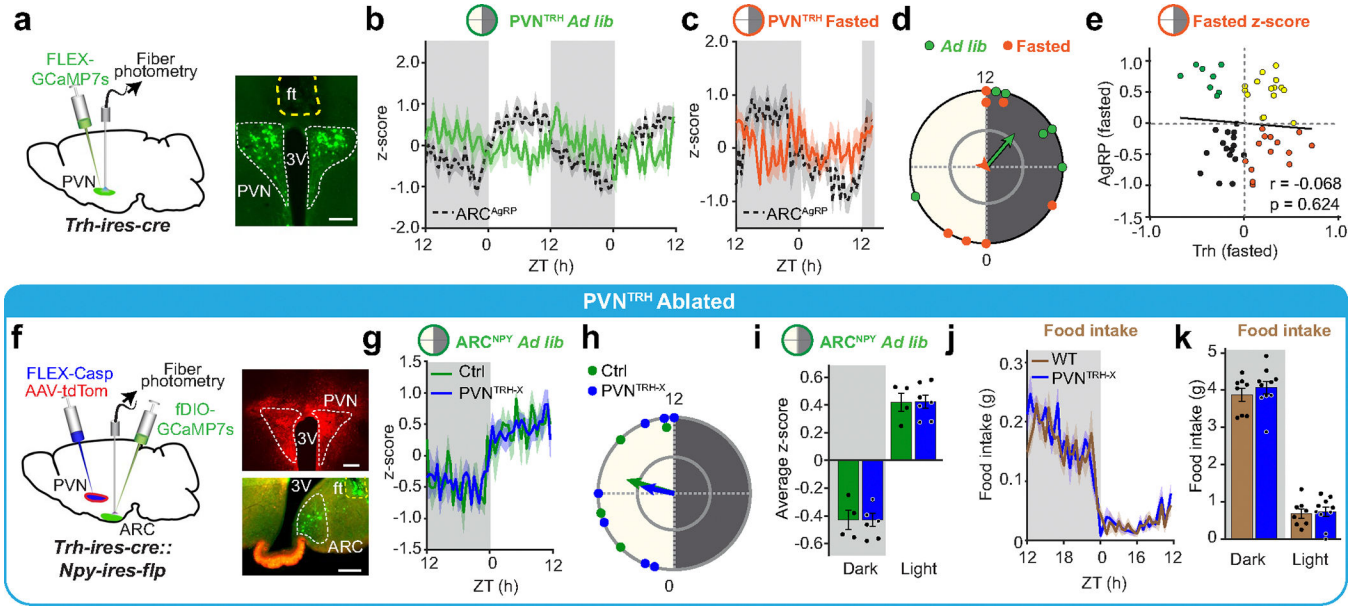

Extended Data Fig. 5 |. Impairing input from PVN^{TRH} does not affect rhythms for feeding and AgRP activity.

a. Schematic and representative image of *in vivo* fiber photometry recording of TRH neuronal Ca^{2+} activity in PVN. ft: Fiber tract. Scale: 300 μm. **b,c**. Average PVN^{TRH} Ca^{2+} activity overlaid with AgRP-neuron activity (from Fig. 1) in *AL* (b) and fasted (c) states. n = 6 AL, n = 7 fasted animals. **d**. Rayleigh-plot of PVN^{TRH} activity in *AL* fed (mean peak time ZT14.7, not significant) and fasted (mean peak time at ZT21, not significant) mice. Phases do not differ significantly. **e**. Two-tailed Pearson correlation between average fasted PVN^{TRH} and average AgRP activities. **f**. Schematic of *in vivo* fiber photometry recording from ARC^{NPY} neurons in mice with PVN^{TRH} ablation. Representative images of ARC:GCaMP7s and PVN showing AAV-tdTomato marking the site of caspase injection

(upper scale: 300 μm lower scale: 250 μm). **g**. Average ARC^{NPY} GCaMP activity in animals with PVN^{TRH} ablation (PVN^{TRH-X}) or with intact PVN^{TRH} neurons (Ctrl). Average of 3 days and n = 4 Ctrl and n = 7 PVN^{TRH-X} mice. **h**. Rayleigh-plot of ARC^{NPY} GCaMP activity in PVN^{TRH-X} mice (mean peak at ZT7) versus control (mean peak time at ZT7.08). Phases do not differ significantly between two groups. **i**. Comparison of dark and light phase ARC^{NPY} activity in mice with or without PVN^{TRH} ablation, two-tailed, unpaired t-test, n = 4 ctrl, 7 PVN^{TRH-X} mice. **j,k**. Feeding pattern of PVN^{TRH-X} mice (j, n = 8 Ctrl and 10 PVN^{TRH-X} mice) and total consumed food during daytime and nighttime (k) compared to control animals, two-tailed, unpaired t-test, n = 8 Ctrl and 10 PVN^{TRH-X} mice. Data are presented as mean ± SEM. For exact P-values and statistics, see Extended Data Fig. 5 Source Data.

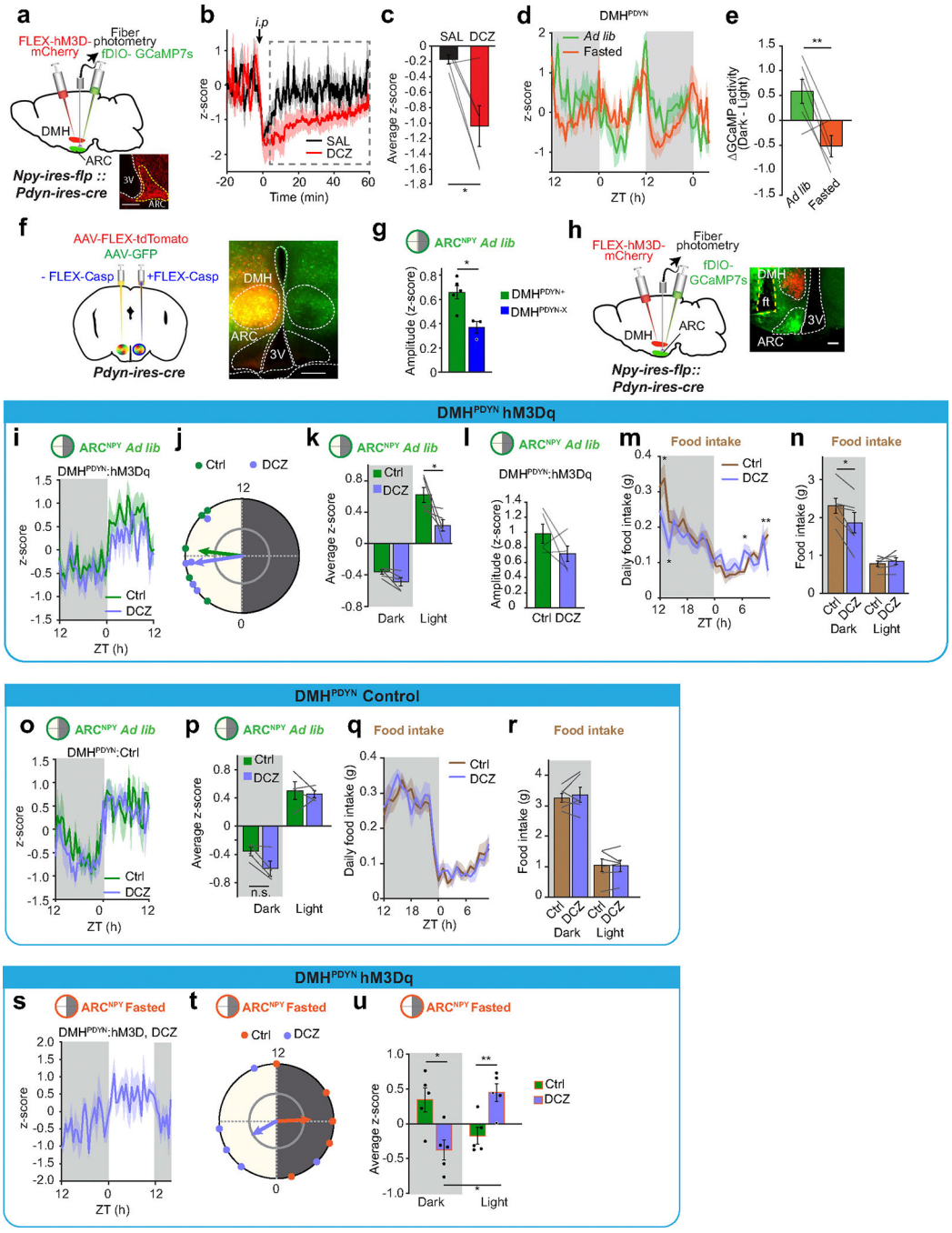

Extended Data Fig. 6 |. Rhythmic activity of DMH^{PDYN} is altered by food access.

a. Schematic of *in vivo* fiber photometry recording from ARC^{NPY} neurons in mice whose DMH^{PDYN} neurons have been transduced with *AAV-FLEX-hM3D-mCherry*. **b**. Effect of DMH^{PDYN} neuron activation on ARC^{NPY} calcium response (n = 5 mice). **c**. Average ARC^{NPY} activity in squared period (b) after saline (SAL) or DCZ injection (two-tailed paired t-test, *p = 0.028, n = 5 mice). **d**. *In vivo* DMH^{PDYN} neuron activities in *AL* and fasted mice (6 mice). **e**. Difference in average DMH^{PDYN} neuron activity in dark (ZT14–20) and light (ZT2–8) phases in *AL* and fasted mice (n = 6 mice, two-tailed paired t-test,

p = 0.005). **f. Schematic and representative image of caspase ablation of DMH^{PDYN} neurons (DMH^{PDYN-X}). **g**. Circadian amplitude of ARC$^{NPY/AGRP}$ activity in intact (n = 5) and DMH^{PDYN-X} mice (n = 3, two-tailed unpaired t-test, *p = 0.013). **h**. Schematic and representative image of *in vivo* fiber photometry recording from ARC^{NPY} neurons in mice with chronic DMH^{PDYN} activation. Scale: 200 μm **i**. Average ARC^{NPY} activity in mice that received DCZ in their drinking water versus control mice (Ctrl: no DCZ, average of 2 days, n = 5 mice each). **j**. Rayleigh-plot of ARC^{NPY} activity (DCZ mean peak: ZT5.4, Rayleigh p = 0.0123, Ctrl mean peak: ZT6.4, Rayleigh p = 0.0417, phases do not differ significantly). **k**. Average ARC^{NPY} activity for dark and light phases, two-tailed, paired t-test, *p = 0.012, n = 5 mice. **l**. Circadian amplitude of ARC^{NPY} activity in control and DCZ groups (n = 5 mice each). **m,n**. Daily feeding pattern (m, DCZ vs Ctrl *p < 0.05, **p = 0.0036, 5-days average, n = 6 mice each) and total food intake (n, two-tailed, paired t-test, * p = 0.017, 5-days average, n = 6 mice each). **o-r**. Same as i,k,m,n, but with mice without viral DREADD injection (n = 4 mice each). **s**. ARC^{NPY} activity in DCZ group fasted at ZT11 (n = 5 mice). **t**. Rayleigh-plots showing peak time in fasted control and DCZ mice (Control mean peak: ZT17.81, DCZ: ZT4.04, phases differ significantly, p = 0.0154, circular one-way ANOVA). **u**. Average dark and light time ARC^{NPY} activity in fasted control and DCZ groups (n = 5 mice, two-tailed, unpaired t-test, *p < 0.03, **p = 0.007. Data are presented as mean ± SEM. For exact P-values, and statistics, see Extended Data Fig. 6 Source Data.

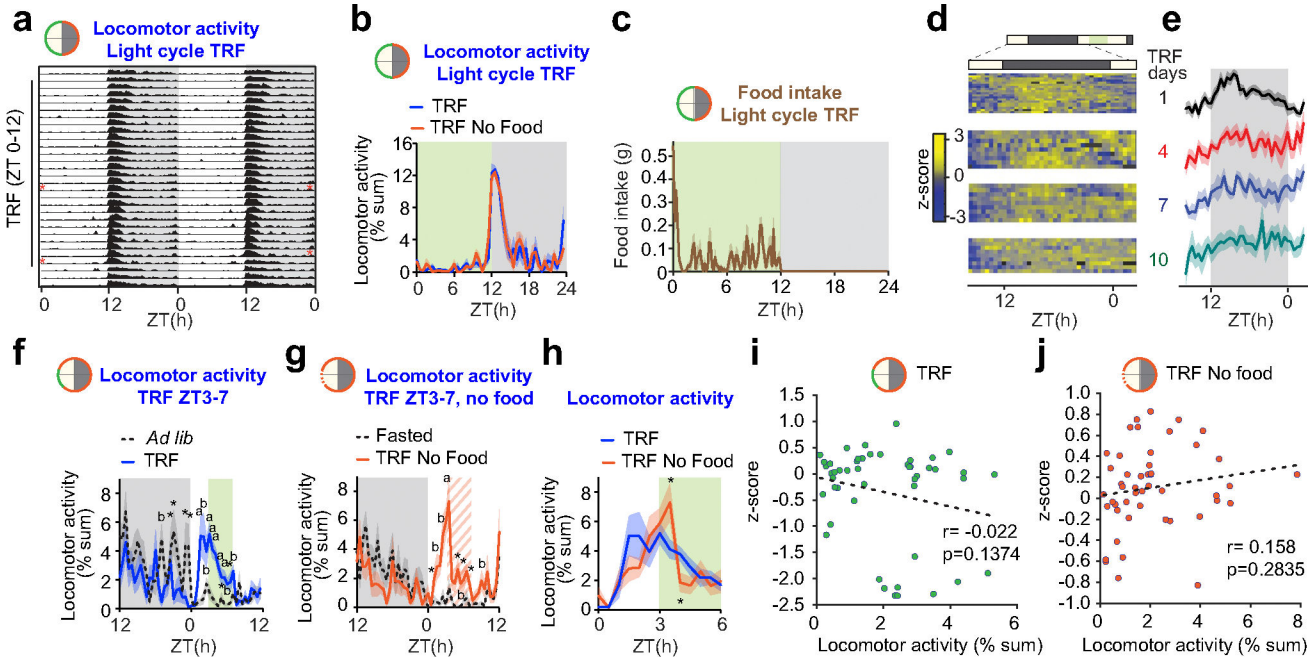

Extended Data Fig. 7 |. Time restricted food access synchronizes AgRP-neuron activity rhythms. **a,b**. Average daily actogram (a) and average locomotor activity graph on TRF days 23 and no food access day 24 (b) in animals that were given restricted access to food only during daytime (ZT0–12). Orange* denotes fasted days. **c**. Food intake on day 23 in animals going through daytime TRF. **d,e**. Nighttime surge in AgRP GCaMP activity dynamics in each mouse shown as heatmap (d) and on average (e) on TRF days 1, 4, 7 and 10 (n = 19, 9, 10, 9 animals, respectively) where animals had access to food between ZT3–7. **f**. Average

locomotor activity in mice under TRF regimen (day 10) compared to *AL* animals (n = 10 TRF,15 *AL* mice. Two-tailed unpaired t-test, * $p < 0.05$, [b] $p < 0.01$, [a] $p < 0.001$). **g**. Same as f, but TRF day 11 without food access is compared to fasted animals on otherwise *AL* schedule (n = 10 mice each). **h**. Average locomotor activity around food access time at ZT3 in animals on TRF day 10 and day 11 without food access (n = 10 mice, two-tailed paired t-test, ZT3.5 *p = 0.043, ZT4 *p = 0.038). **i,j**. Two-tailed Pearson correlation of AgRP GCaMP activity (z-score) and locomotor activity in animals on TRF day 10 (i) and day 11 without food access (j). Data are presented as mean ± SEM. for exact P values, see Extended Data 7 Source Data.

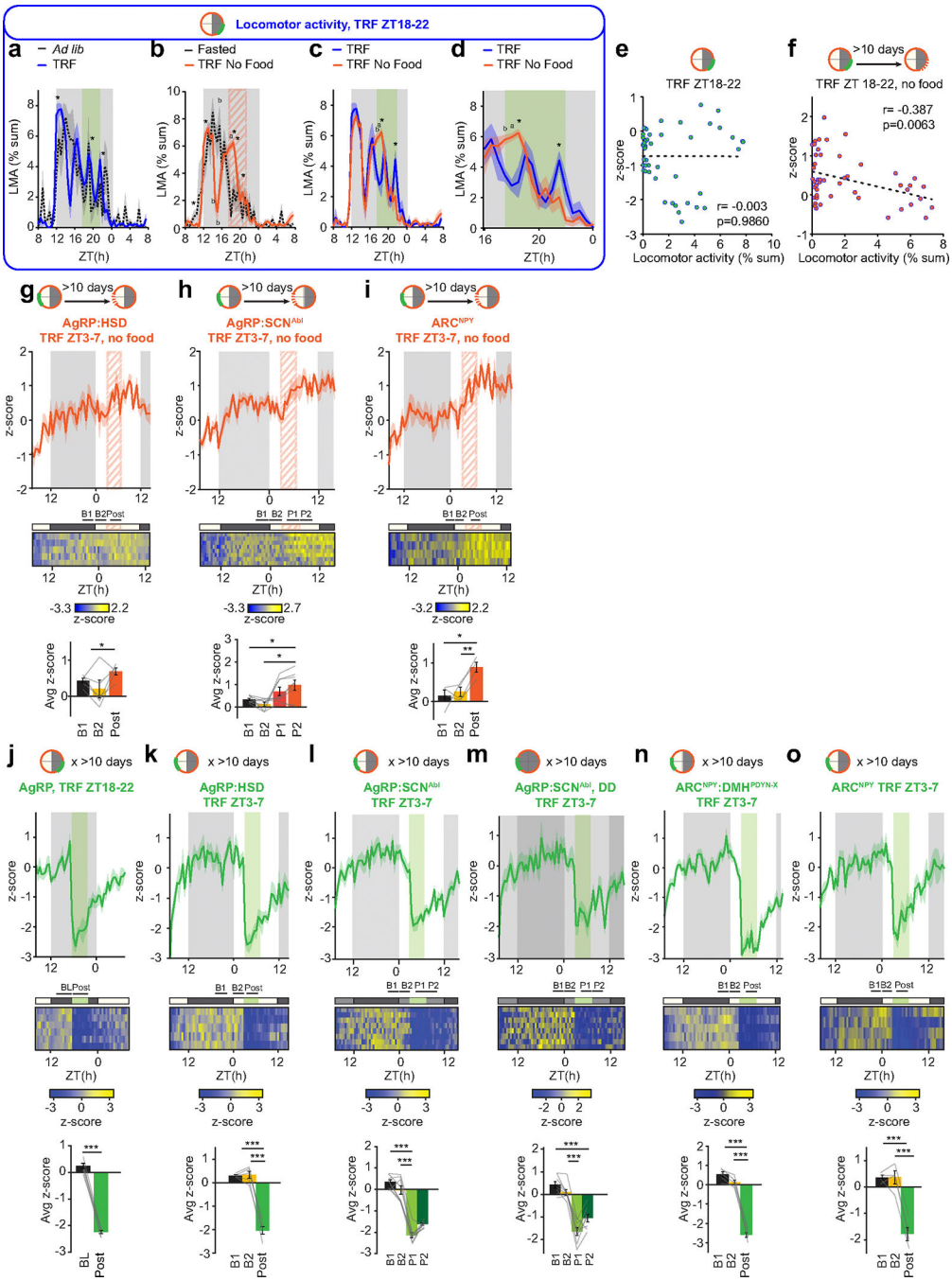

Extended Data Fig. 8 |. Time restricted food access alters AgRP-neuron activity rhythms.

a. Average locomotor activity in mice under TRF regimen (day-17), where animals had access to food between ZT18–22, compared to their *AL* days (n = 7 animals, two-tailed paired t-test, *p < 0.05). **b**. Same as a, but TRF day-18 without food access is compared to fasted days while on *AL* schedule (*p < 0.05, ^{b}p < 0.01, ^{a}p < 0.001). **c,d**. Overlaid average locomotor activities during 24-h (c) and around food access time at ZT18 (d) in animals on TRF with and without food access (n = 7 mice, two-tailed paired t-test, *p < 0.05, ^{b}p < 0.01, ^{a}p < 0.001). **e,f**. Two-tailed Pearson correlation of AgRP GCaMP activity

and locomotor activity in animals on TRF day-17 (e) and day-18 without food access (f). **g-i**. AgRP (g,h) and ARC^{NPY} (i) neuron activities recorded from 11βHSD2 expressing (g), SCN-ablated (h) and WT control (i) mice subjected to TRF between ZT3–7 for more than 10 days and was provided no food during the recording period. Upper panels: average of n = 5 (g), n = 8 (h) and n = 4 (i) mice, middle panels: individual data from each animal, lower panels: comparison of AgRP/NPY activity in BL-1 (before light phase, ZT21–0), BL-2 (light onset, before food, ZT0-ZT3) and post-food time (Post or P1, ZT4–7), or P2 (ZT7–10, h) periods. One-way ANOVA followed by Tukey multiple comparison test. *p < 0.05, **p < 0.01 **j**. AgRP-neuron activity recorded from mice that had been subjected to TRF between ZT18–22 for 17 days. Upper panel: average of n = 6 animals, middle panel: individual data from each animal, lower panel: AgRP activity in BL (ZT15–17.5) and post-food time (ZT19–22) periods ***p < 0.0001. Green shades depict food availability. **k-o**. AgRP (k-m) and ARC^{NPY} (n,o) neuron activities recorded from 11βHSD2 expressing (k), SCN-ablated (l), SCN-ablated, under DD conditions (m), DMH^{PDYN}-ablated (n) and intact control (o) mice that had been subjected to TRF between ZT3–7 for more than 10 days. Upper panels: average of n = 5 (k,n), n = 8 (l,m) and n = 4 (o) mice; middle and lower panels: same as in g-i, ***p < 0.001). Data are presented as mean ± SEM. For exact P-values, see Extended Data 8 Source Data.

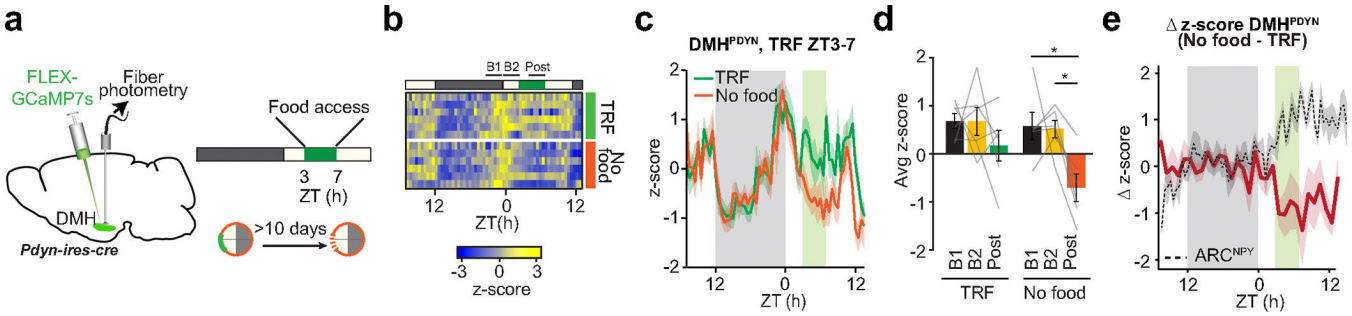

Extended Data Fig. 9 |. DMH^{PDYN} neurons provide timed disinhibition to AgRP-neurons in TRF.

a. Left: Schematic of *in vivo* fiber photometry recording of PDYN neuronal Ca^{2+} activity in DMH. Right: Diagram describing TRF setting. **b,c**. Heatmap showing individual (b) and line graph showing averaged (c) DMH^{PDYN} activity in mice under TRF between ZT3–7. n = 6 mice. **d**. Average DMH^{PDYN} activity in B1 (ZT21–0), B2(ZT0–3) and Post (ZT4–7) periods in TRF and no food access days. Two-way ANOVA with Tukey's multiple comparison analysis (No food, B1 vs Post, p = 0.012, B2 vs Post p = 0.016, n = 6 mice). **e**. Change in DMH^{PDYN} activity (Δ = z-score on TRF day – z-score on no food access day from c) overlaid with ARC$^{NPY/AgRP}$ (from Extended Data Figure 8i). Data are presented as mean ± SEM. For exact P values and data, see Extended Data 9 Source Data.

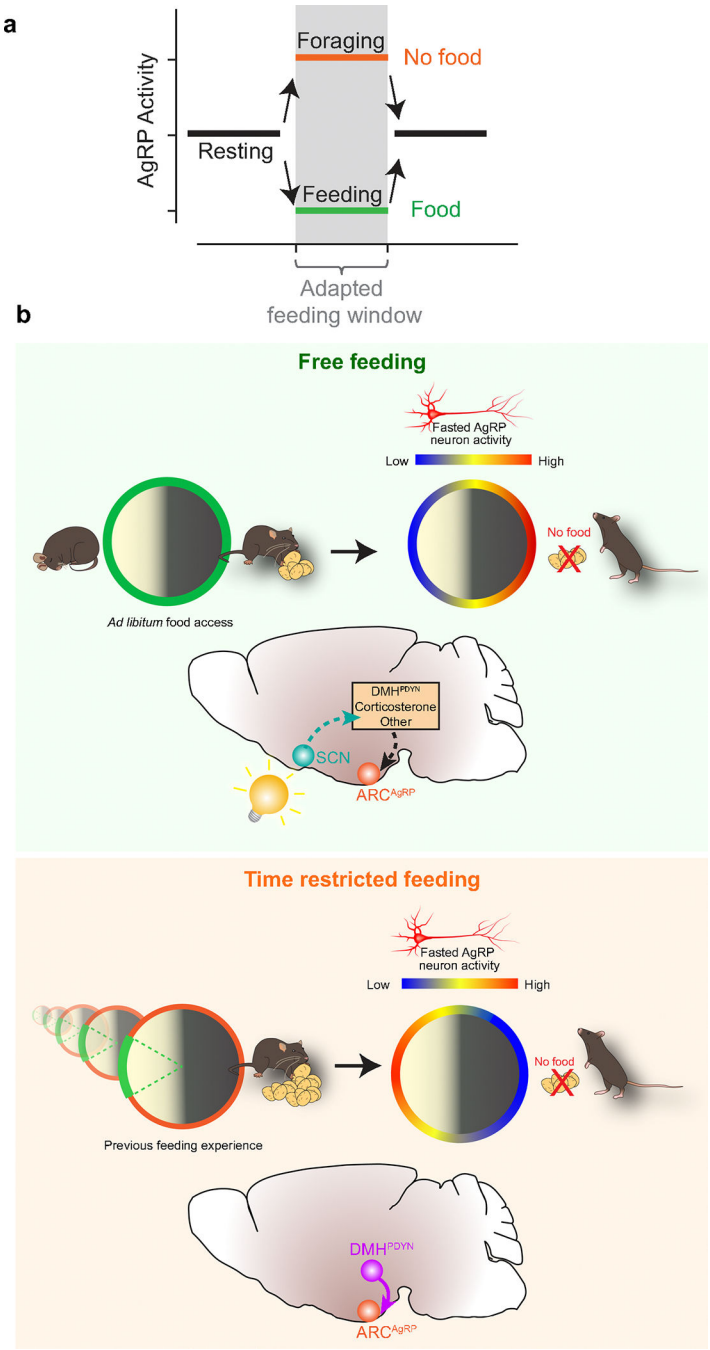

Extended Data Fig. 10 |. Allostatic regulation of AgRP-neuron activity by past circadian feeding experience.

a. Proposed model for daily fluctuations in relative AgRP-neuron activity levels. Outside of feeding window, AgRP-neuron activity is relatively unaffected by feeding status (at least on the first day in food deprivation), whereas during feeding time the activity is highly sensitive to food availability. The ‘Adapted feeding window’ is the time of day during which feeding periodically occurred in previous days. In free feeding mice, this window is dark phase and synchronized by light; however, it can be dissociated from circadian phase and reset by restricted food access. **b**. Schematic depiction of long-term regulation

of AgRP-neuron activity by previous day's circadian feeding experience. Feeding time is encoded into AgRP-neuron activity such that activity rises if anticipated food access does not occur. Top: Under free feeding conditions, AgRP-neuron activity directly or indirectly synchronizes to light through a process that requires intact SCN. Bottom: In time restricted feeding, AgRP activity uncouples from light and synchronizes to feeding time in a process that required intact DMH input.

Supplementary Material

Refer to Web version on PubMed Central for supplementary material.

Acknowledgements

This work is supported by National Institutes of Health grant R01DK126740 to D.A. We thank E. Herzog, S. Sternson and K. Rahmouni for feedback on the paper and J. Resch for providing the 11βHSD2 virus.

Data availability

Raw data are available from the corresponding author upon reasonable request. Source data are provided with this paper.

References

1. Mistlberger RE Food as circadian time cue for appetitive behavior. F1000Res. 9, F1000 Faculty Rev-61 (2020).
2. Gooley JJ, Schomer A & Saper CB The dorsomedial hypothalamic nucleus is critical for the expression of food-entrainable circadian rhythms. Nat. Neurosci. 9, 398–407 (2006). [PubMed: 16491082]
3. Crosby P et al. Insulin/IGF-1 drives PERIOD synthesis to entrain circadian rhythms with feeding time. Cell 177, 896–909.e20 (2019). [PubMed: 31030999]
4. Landgraf D et al. Oxyntomodulin regulates resetting of the liver circadian clock by food. eLife 4, e06253 (2015). [PubMed: 25821984]
5. Balsalobre A et al. Resetting of circadian time in peripheral tissues by glucocorticoid signaling. Science 289, 2344–2347 (2000). [PubMed: 11009419]
6. LeSauter J, Hoque N, Weintraub M, Pfaff DW & Silver R Stomach ghrelin-secreting cells as food-entrainable circadian clocks. Proc. Natl Acad. Sci. USA 106, 13582–13587 (2009). [PubMed: 19633195]
7. Gallardo CM et al. Dopamine receptor 1 neurons in the dorsal striatum regulate food anticipatory circadian activity rhythms in mice. eLife 3, e03781 (2014). [PubMed: 25217530]
8. Deem JD, Faber CL & Morton GJ AgRP neurons: regulators of feeding, energy expenditure, and behavior. FEBS J. 289, 2362–2381 (2021). [PubMed: 34469623]
9. Chen Y, Lin Y-C, Kuo T-W & Knight ZA Sensory detection of food rapidly modulates arcuate feeding circuits. Cell 160, 829–841 (2015). [PubMed: 25703096]
10. Podyma B et al. The p75 neurotrophin receptor in AgRP neurons is necessary for homeostatic feeding and food anticipation. eLife 9, e52623 (2020). [PubMed: 31995032]
11. Tan K, Knight ZA & Friedman JM Ablation of AgRP neurons impairs adaption to restricted feeding. Mol. Metab. 3, 694–704 (2014). [PubMed: 25352998]
12. Bugarith K, Dinh TT, Li A-J, Speth RC & Ritter S Basomedial hypothalamic injections of neuropeptide Y conjugated to saporin selectively disrupt hypothalamic controls of food intake. Endocrinology 146, 1179–1191 (2005). [PubMed: 15604214]

13. Reichenbach A et al. AgRP neurons require carnitine acetyltransferase to regulate metabolic flexibility and peripheral nutrient partitioning. Cell Rep. 22, 1745–1759 (2018). [PubMed: 29444428]
14. Cedernaes J et al. Transcriptional basis for rhythmic control of hunger and metabolism within the AgRP neuron. Cell Metab. 29, 1078–1091 (2019). [PubMed: 30827863]
15. Henry FE, Sugino K, Tozer A, Branco T & Sternson SM Cell type-specific transcriptomics of hypothalamic energy-sensing neuron responses to weight-loss. eLife 4, e09800 (2015). [PubMed: 26329458]
16. Mandelblat-Cerf Y et al. Arcuate hypothalamic AgRP and putative POMC neurons show opposite changes in spiking across multiple timescales. eLife 4, e07122 (2015). [PubMed: 26159614]
17. Betley JN et al. Neurons for hunger and thirst transmit a negative-valence teaching signal. Nature 521, 180–185 (2015). [PubMed: 25915020]
18. Su Z, Alhadeff AL & Betley JN Nutritive, post-ingestive signals are the primary regulators of AgRP neuron activity. Cell Rep. 21, 2724–2736 (2017). [PubMed: 29212021]
19. Atasoy D, Aponte Y, Su HH & Sternson SM A FLEX switch targets Channelrhodopsin-2 to multiple cell types for imaging and long-range circuit mapping. J. Neurosci. 28, 7025–7030 (2008). [PubMed: 18614669]
20. Savontaus E, Conwell IM & Wardlaw SL Effects of adrenalectomy on AGRP, POMC, NPY and CART gene expression in the basal hypothalamus of fed and fasted rats. Brain Res. 958, 130–138 (2002). [PubMed: 12468037]
21. Lu X-Y et al. Diurnal rhythm of agouti-related protein and its relation to corticosterone and food intake. Endocrinology 143, 3905–3915 (2002). [PubMed: 12239102]
22. Gyengesi E et al. Corticosterone regulates synaptic input organization of POMC and NPY/AgRP neurons in adult mice. Endocrinology 151, 5395–5402 (2010). [PubMed: 20843996]
23. Perry RJ et al. Leptin's hunger-suppressing effects are mediated by the hypothalamic-pituitary-adrenocortical axis in rodents. Proc. Natl Acad. Sci. USA 116, 13670–13679 (2019). [PubMed: 31213533]
24. Geerling JC, Engeland WC, Kawata M & Loewy AD Aldosterone target neurons in the nucleus tractus solitarius drive sodium appetite. J. Neurosci. 26, 411–417 (2006). [PubMed: 16407537]
25. Broberger C, Johansen J, Johansson C, Schalling M & Hokfelt T The neuropeptide Y/agouti gene-related protein (AGRP) brain circuitry in normal, anorectic, and monosodium glutamate-treated mice. Proc. Natl Acad. Sci. USA 95, 15043–15048 (1998). [PubMed: 9844012]
26. Krashes MJ et al. An excitatory paraventricular nucleus to AgRP neuron circuit that drives hunger. Nature 507, 238–242 (2014). [PubMed: 24487620]
27. Garfield AS et al. Dynamic GABAergic afferent modulation of AgRP neurons. Nat. Neurosci. 19, 1628–1635 (2016). [PubMed: 27643429]
28. Kim ER et al. Paraventricular hypothalamus mediates diurnal rhythm of metabolism. Nat. Commun. 11, 3794 (2020). [PubMed: 32732906]
29. Stephan FK & Becker G Entrainment of anticipatory activity to various durations of food access. Physiol. Behav. 46, 731–741 (1989). [PubMed: 2602500]
30. Honma KI, Honma S & Hiroshige T Feeding-associated corticosterone peak in rats under various feeding cycles. Am. J. Physiol. 246, R721–R726 (1984). [PubMed: 6720996]
31. Fuller PM, Lu J & Saper CB Differential rescue of light- and food-entrainable circadian rhythms. Science 320, 1074–1077 (2008). [PubMed: 18497298]
32. Angeles-Castellanos M, Aguilar-Roblero R & Escobar C c-Fos expression in hypothalamic nuclei of food-entrained rats. Am. J. Physiol. Regul. Integr. Comp. Physiol. 286, R158–R165 (2004). [PubMed: 12933360]
33. Mieda M, Williams SC, Richardson JA, Tanaka K & Yanagisawa M The dorsomedial hypothalamic nucleus as a putative food-entrainable circadian pacemaker. Proc. Natl Acad. Sci. USA 103, 12150–12155 (2006). [PubMed: 16880388]
34. Atasoy D, Betley JN, Su HH & Sternson SM Deconstruction of a neural circuit for hunger. Nature 488, 172–177 (2012). [PubMed: 22801496]

35. Aponte Y, Atasoy D & Sternson SM AGRP neurons are sufficient to orchestrate feeding behavior rapidly and without training. Nat. Neurosci. 14, 351–355 (2011). [PubMed: 21209617]
36. Krashes MJ et al. Rapid, reversible activation of AgRP neurons drives feeding behavior in mice. J. Clin. Invest. 121, 1424–1428 (2011). [PubMed: 21364278]
37. Goldstein N et al. Hypothalamic neurons that regulate feeding can influence sleep/wake states based on homeostatic need. Curr. Biol. 28, 3736–3747.e3 (2018). [PubMed: 30471995]
38. Buijs FN et al. Suprachiasmatic nucleus interaction with the arcuate nucleus; essential for organizing physiological rhythms. eNeuro 4, ENEURO.0028–17.2017 (2017).
39. Mendez-Hernandez R, Escobar C & Buijs RM Suprachiasmatic nucleus-arcuate nucleus axis: interaction between time and metabolism essential for health. Obesity 28, S10–S17 (2020). [PubMed: 32538539]
40. Ohta H, Yamazaki S & McMahon DG Constant light desynchronizes mammalian clock neurons. Nat. Neurosci. 8, 267–269 (2005). [PubMed: 15746913]
41. Chou TC et al. Critical role of dorsomedial hypothalamic nucleus in a wide range of behavioral circadian rhythms. J. Neurosci. 23, 10691–10702 (2003). [PubMed: 14627654]
42. Kalsbeek A et al. GABA receptors in the region of the dorsomedial hypothalamus of rats are implicated in the control of melatonin and corticosterone release. Neuroendocrinology 63, 69–78 (1996). [PubMed: 8839357]
43. Tso CF et al. Astrocytes regulate daily rhythms in the suprachiasmatic nucleus and behavior. Curr. Biol. 27, 1055–1061 (2017). [PubMed: 28343966]
44. Damiola F et al. Restricted feeding uncouples circadian oscillators in peripheral tissues from the central pacemaker in the suprachiasmatic nucleus. Genes Dev. 14, 2950–2961 (2000). [PubMed: 11114885]
45. Stephan FK, Swann JM & Sisk CL Anticipation of 24-hr feeding schedules in rats with lesions of the suprachiasmatic nucleus. Behav. Neural Biol. 25, 346–363 (1979). [PubMed: 464979]
46. Patton DF & Mistlberger RE Circadian adaptations to meal timing: neuroendocrine mechanisms. Front. Neurosci. 7, 185 (2013). [PubMed: 24133410]
47. Faber CL et al. Leptin receptor neurons in the dorsomedial hypothalamus regulate diurnal patterns of feeding, locomotion, and metabolism. eLife 10, e63671 (2021). [PubMed: 33527893]
48. Tang Q et al. Leptin receptor neurons in the dorsomedial hypothalamus input to the circadian feeding network. Sci. Adv. 9, eadh9570 (2023). [PubMed: 37624889]
49. Luby MD et al. Food anticipatory activity behavior of mice across a wide range of circadian and non-circadian intervals. PLoS ONE 7, e37992 (2012). [PubMed: 22662260]
50. Reichenbach A et al. Carnitine acetyltransferase (Crat) in hunger-sensing AgRP neurons permits adaptation to calorie restriction. FASEB J. 32, fj201800634R (2018).
51. Reed F, Lockie SH, Reichenbach A, Foldi CJ & Andrews ZB Appetite to learn: an allostatic role for AgRP neurons in the maintenance of energy balance. Curr. Opin. Endocr. Metab. Res. 24, 100337 (2022).
52. Sterling P Allostasis: a model of predictive regulation. Physiol. Behav. 106, 5–15 (2012). [PubMed: 21684297]
53. Ramsay DS & Woods SC Clarifying the roles of homeostasis and allostasis in physiological regulation. Psychol. Rev. 121, 225–247 (2014). [PubMed: 24730599]
54. Zhang Q et al. Food-induced dopamine signaling in AgRP neurons promotes feeding. Cell Rep. 41, 111718 (2022). [PubMed: 36450244]
55. Grove JCR et al. Dopamine subsystems that track internal states. Nature 608, 374–380 (2022). [PubMed: 35831501]
56. Reichenbach A et al. Metabolic sensing in AgRP neurons integrates homeostatic state with dopamine signalling in the striatum. eLife 11, e72668 (2022). [PubMed: 35018884]
57. He Z et al. Cellular and synaptic reorganization of arcuate NPY/AgRP and POMC neurons after exercise. Mol. Metab. 18, 107–119 (2018). [PubMed: 30292523]
58. Hatori M et al. Time-restricted feeding without reducing caloric intake prevents metabolic diseases in mice fed a high-fat diet. Cell Metab. 15, 848–860 (2012). [PubMed: 22608008]

59. Chaix A, Zarrinpar A, Miu P & Panda S Time-restricted feeding is a preventative and therapeutic intervention against diverse nutritional challenges. Cell Metab. 20, 991–1005 (2014). [PubMed: 25470547]

60. Acosta-Rodriguez VA, Rijo-Ferreira F, Green CB & Takahashi JS Importance of circadian timing for aging and longevity. Nat. Commun. 12, 2862 (2021). [PubMed: 34001884]

61. Matikainen-Ankney BA et al. An open-source device for measuring food intake and operant behavior in rodent home-cages. eLife 10, e66173 (2021). [PubMed: 33779547]

62. Aklan I et al. NTS catecholamine neurons mediate hypoglycemic hunger via medial hypothalamic feeding pathways. Cell Metab. 31, 313–326.e5 (2020). [PubMed: 31839488]

63. Jones JR, Simon T, Lones L & Herzog ED SCN VIP neurons are essential for normal light-mediated resetting of the circadian system. J. Neurosci. 38, 7986–7995 (2018). [PubMed: 30082421]

64. Jones JR, Chaturvedi S, Granados-Fuentes D & Herzog ED Circadian neurons in the paraventricular nucleus entrain and sustain daily rhythms in glucocorticoids. Nat. Commun. 12, 5763 (2021). [PubMed: 34599158]

65. Berens P CircStat: a MATLAB toolbox for circular statistics. J. Stat. Softw. 31, 1–21 (2009).

66. Hughes ME, Hogenesch JB & Kornacker K JTK_CYCLE: an efficient nonparametric algorithm for detecting rhythmic components in genome-scale data sets. J. Biol. Rhythms 25, 372–380 (2010). [PubMed: 20876817]

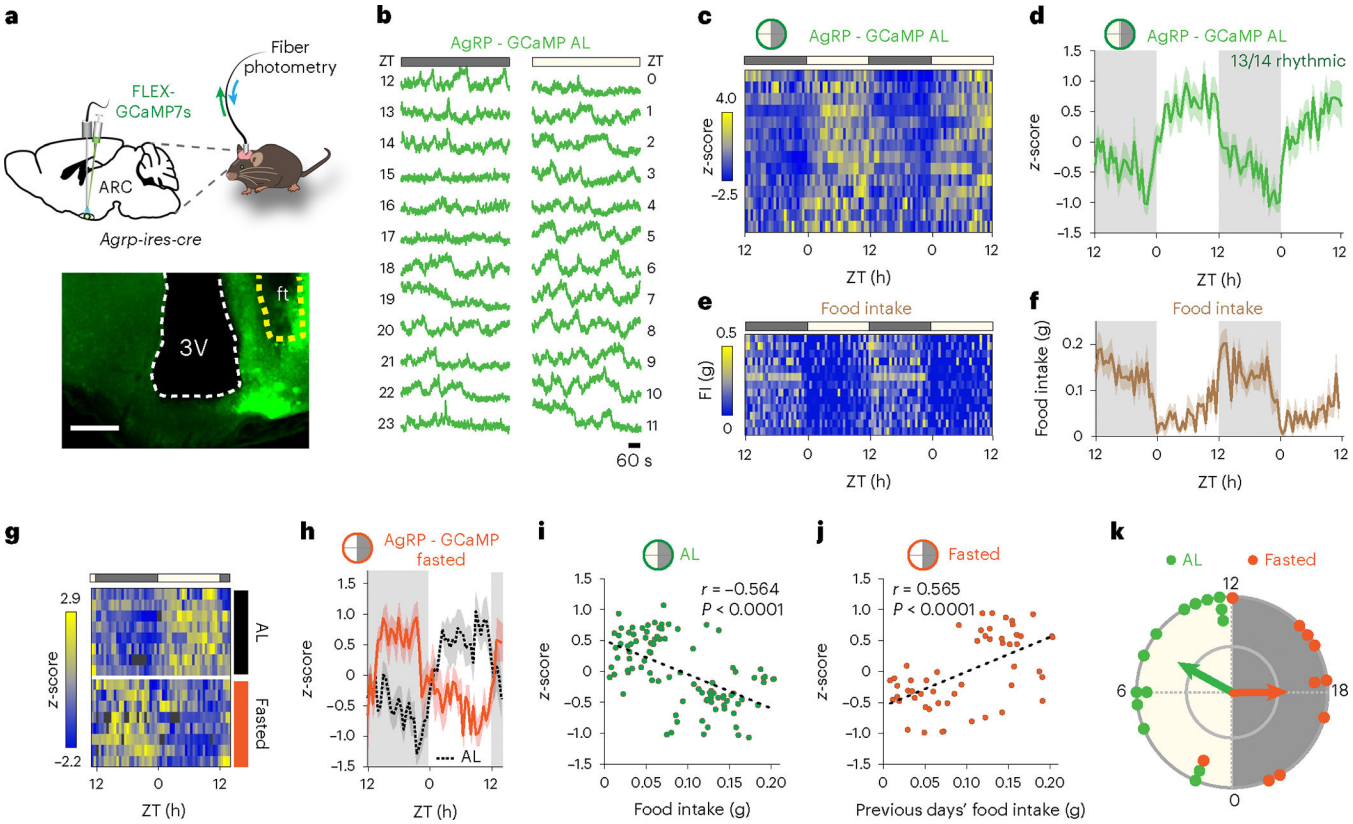

Fig. 1 |. ARC^{AgRP}-neuron activity exhibits daily rhythms.

a, Schematic of in vivo fiber photometry recording of AgRP-neuronal Ca^{2+} activity in the ARC in *Agrp-ires-cre* mice (upper panel). Lower panel, representative image showing GCaMP7s-expressing AgRP neurons and fiber tract (ft). Scale bar, 200 μm. **b**, Representative hourly GCaMP7s traces (*z*-score) from AgRP neurons recorded for 10 min at every 30 min in LD (12 h light, 12 h dark). White bar: light phase; dark gray bar: dark phase. **c**, Heat map showing AgRP GCaMP7s activity rhythms of each mouse/row recorded in LD. **d**, Averaged rhythms (n = 13 of 14 mice were rhythmic, JTK cycle, P < 0.02 or less) for 2 d. Dark shade: dark phase; no shade: light phase. **e**,**f**, Heat map showing daily rhythm of food intake by each animal in LD (**e**) and averaged 2-d food intake (**f**). **g**, Heat maps showing AgRP-neuron activity of each mouse in AL (upper) and fasted (lower, started at ZT11) conditions. **h**, Averaged AgRP GCaMP7s rhythms in fasted conditions overlaid with AL (n = 10 animals). **i**,**j**, Two-tailed Pearson correlation between average food intake and average AgRP-neuron activity from AL feeding mice (14 animals) (**i**) and from mice fasted starting on the subsequent day's late afternoon (ZT11, 10 animals) (**j**) across the same circadian timepoints. Previous days' food intake averages were used for the correlation of fasted data. **k**, Rayleigh plots of AgRP rhythms in AL (peak times averaging at ZT7.92, shown by green arrow, Rayleigh P = 0.0018) and fasted (mean peak time at ZT17.93, shown by orange arrow, Rayleigh P = 0.0297) conditions. Phases differ significantly between AL and fasted conditions (circular one-way ANOVA, P < 0.0001) (n = 10 fasted and 14 AL fed animals). Data are presented as mean ± s.e.m. For exact P values and statistics, see Fig. 1 Source Data. FI, food intake.

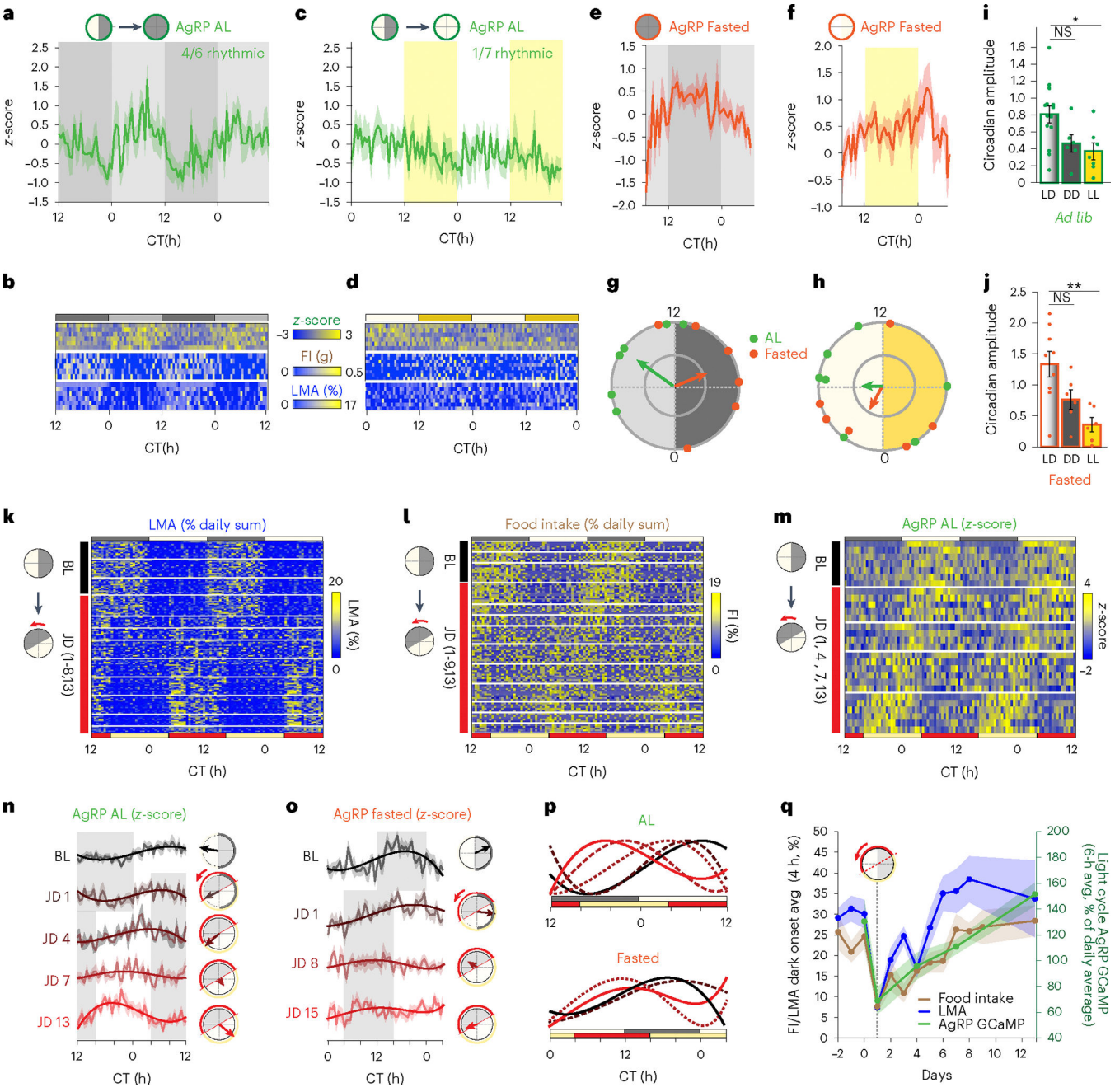

Fig. 2 |. AgRP-neuron activity rhythm is synchronized to light in free-feeding mice.

a,**b**, AgRP-neuron activity rhythm (**a**) in constant dark (DD), with four of six animals still preserving rhythmic activity ($P < 0.01$, JTK cycle) and heat maps (**b**) showing average 2-d AgRP GCaMP7s activity (upper panel), food intake (middle panel) and locomotor activity (LMA, lower panel) of individual animals in DD. Dark gray/yellow shade: subjective nighttime; light gray shade: subjective daytime. **c**,**d**, Same as in **a**,**b**, except in constant light (LL) (one of seven mice rhythmic, $P < 0.0001$, JTK cycle). **e**,**f**, Averaged AgRP-neuron activity rhythm in fasted animals in DD (**e**) and LL (**f**) settings. **g**, Rayleigh plots of AgRP rhythms in AL (mean peak: ZT8.38, $P = 0.0319$, $n = 6$ mice) and fasted (mean peak:

ZT16.52, not significant, $n = 6$ mice) in DD. Circular one-way ANOVA of AL versus fasted phases, $P = 0.0099$. **h**, Rayleigh plots of AgRP rhythms in AL (mean peak: ZT6.04, not significant, $n = 7$ mice) and fasted (mean peak: ZT1.89, not significant, $n = 6$ mice) in LL. Phases do not differ significantly. **i**,**j**, Amplitude of AgRP circadian rhythms (|mean z-score$_{(\text{dark period})}$ − mean z-score$_{(\text{light period})}$|) in AL (**i**) and fasted (**j**) mice ($n = 14$ (LD), $n = 6$ (DD) and $n = 7$ (LL), one-way ANOVA, $^{*}P = 0.0206$ and $^{**}P = 0.0031$). **k**–**m**, Heat maps showing LMA (**k**), food intake (**l**) and AgRP calcium activity (**m**) rhythms shifting from baseline (BL) days (black vertical bar) throughout adaptation to 8-h forward phase shift during jetlag days (JDs, red vertical line, $n = 4$–7 animals). Upper horizontal bars (gray/white) show BL light scheme; lower bars (red/yellow) show jetlag light scheme. **n**,**o**, Shift in AgRP-neuron activity peaks from midday on BL (black line and arrow) to new midday (red line and arrow) throughout JDs (gradient shade lines and arrows) under AL (**n**) and fasted (**o**) conditions. Dark/red rim: BL/jetlag nighttime. **p**, Overlay of fitted average AgRP-neuron activity curves in **n** and **o** for comparison. **q**, Recovery of food intake, daily LMA and AgRP calcium activity (right y axis) from jetlag-induced shift changes. Dark onset: ZT12–ZT16. For AgRP-neuron activity, average activity between ZT1.5 and ZT7.5 on BL and new ZT1.5–ZT7.5 on JDs are shown as percentage of daily average. Jetlag starts on day −1. Data are presented as mean ± s.e.m. For exact n values and statistics, see Fig. 2 Source Data. avg, average; FI, food intake; NS, not significant.

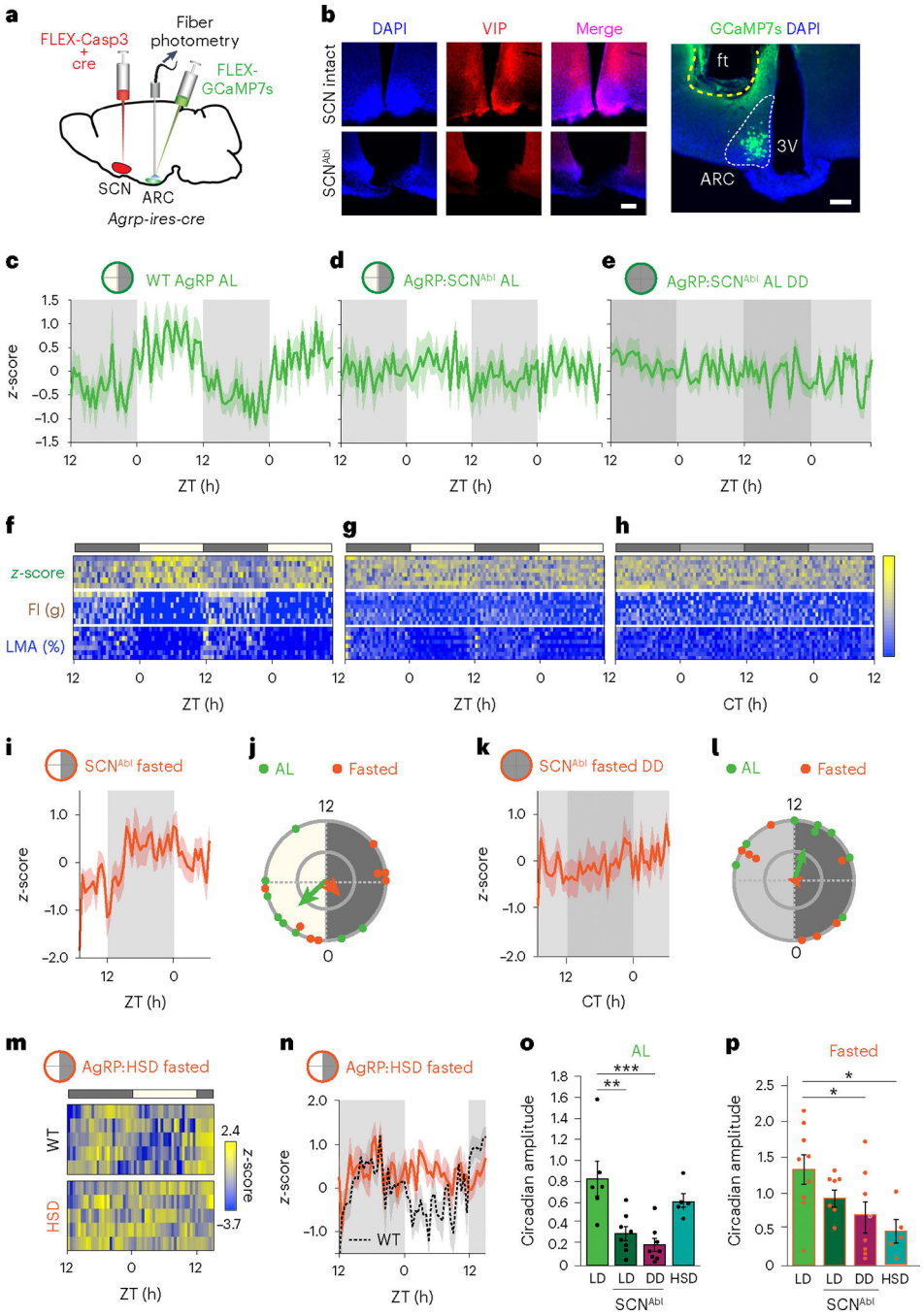

Fig. 3 |. Intact SCN is required for AgRP-neuron activity rhythms in free-feeding mice.

a, Schematic of in vivo fiber photometry recording of AgRP calcium activity in SCN-ablated (SCN^{Abl}) mice. **b**, Representative image showing VIP labeling in the SCN region in intact (upper image) or SCN^{Abl} (lower image) mice and their ARC showing AgRP:GCaMP7s expression. Scale bars, 100 μm. **c**–**e**, Average AgRP GCaMP7s activity rhythms recorded from SCN-intact animals in LD conditions (**c**) ($n = 5$ out of 6 mice rhythmic, JTK cycle, $P < 0.04$), SCN^{Abl} animals in LD conditions (**d**) ($n = 1$ out of 8 mice rhythmic, JTK cycle, $P = 0.0039$) and SCN^{Abl} animals in DD conditions (**e**) ($n = 1$ out of 8 mice rhythmic, JTK cycle,

$P = 0.047$) for 2 d. **f**–**h**, Heat maps showing 2 d of AgRP GCaMP7s (upper panel), food intake (middle panel) and locomotor activity (LMA) (lower panel) of individual SCN-intact animals in LD (**f**), SCN^{Abl} animals in LD (**g**) and SCN^{Abl} animals in DD (**h**). Scale for AgRP GCaMP activity (*z*-score): −4 to +4; for food intake: 0–0.5 g; for actogram: 0–20%. **i**, Averaged (eight mice) AgRP GCaMP7s rhythm in fasted SCN^{Abl} mice in LD. **j**, Rayleigh plots of AgRP rhythms in SCN^{Abl} animals under AL (mean peak: ZT3.14, Rayleigh $P = 0.044$) and fasted (mean peak: ZT21.18, not significant) conditions, in LD. Phases differ significantly between AL and fasted animals (circular one-way ANOVA, $P = 0.0493$, $n = 8$ mice). **k**, Averaged (eight mice) AgRP rhythm in fasted SCN^{Abl} mice in DD. **l**, Rayleigh plots of AgRP rhythms in SCN^{Abl} animals under AL (mean peak: ZT13.15, not significant) and fasted (mean peak: ZT6.82, not significant) conditions, in DD. Phases do not differ significantly ($n = 8$ mice). **m**,**n**, Individual (heat map, **m**) and average (**n**) AgRP GCaMP7s activity rhythms recorded from HSD mice compared to wild-type (WT) mice in fasted conditions. **o**,**p**, Amplitude of circadian rhythms (absolute value of the difference between average AgRP-neuron activity at ZT0–ZT12 and ZT12–ZT0) in AL mice ($n = 6$ LD, $n = 8$ SCN^{Abl} LD and DD, $n = 5$ HSD, one-way ANOVA, **o**) and fasted mice ($n = 9$ LD, $n = 8$ SCN^{Abl} LD and DD, $n = 5$ HSD, one-way ANOVA, **p**). Data are presented as mean ± s.e.m. $*P < 0.05$, $**P < 0.01$ and $***P < 0.001$. For exact *P* values and statistics, see Fig. 3 Source Data. FI, food intake.

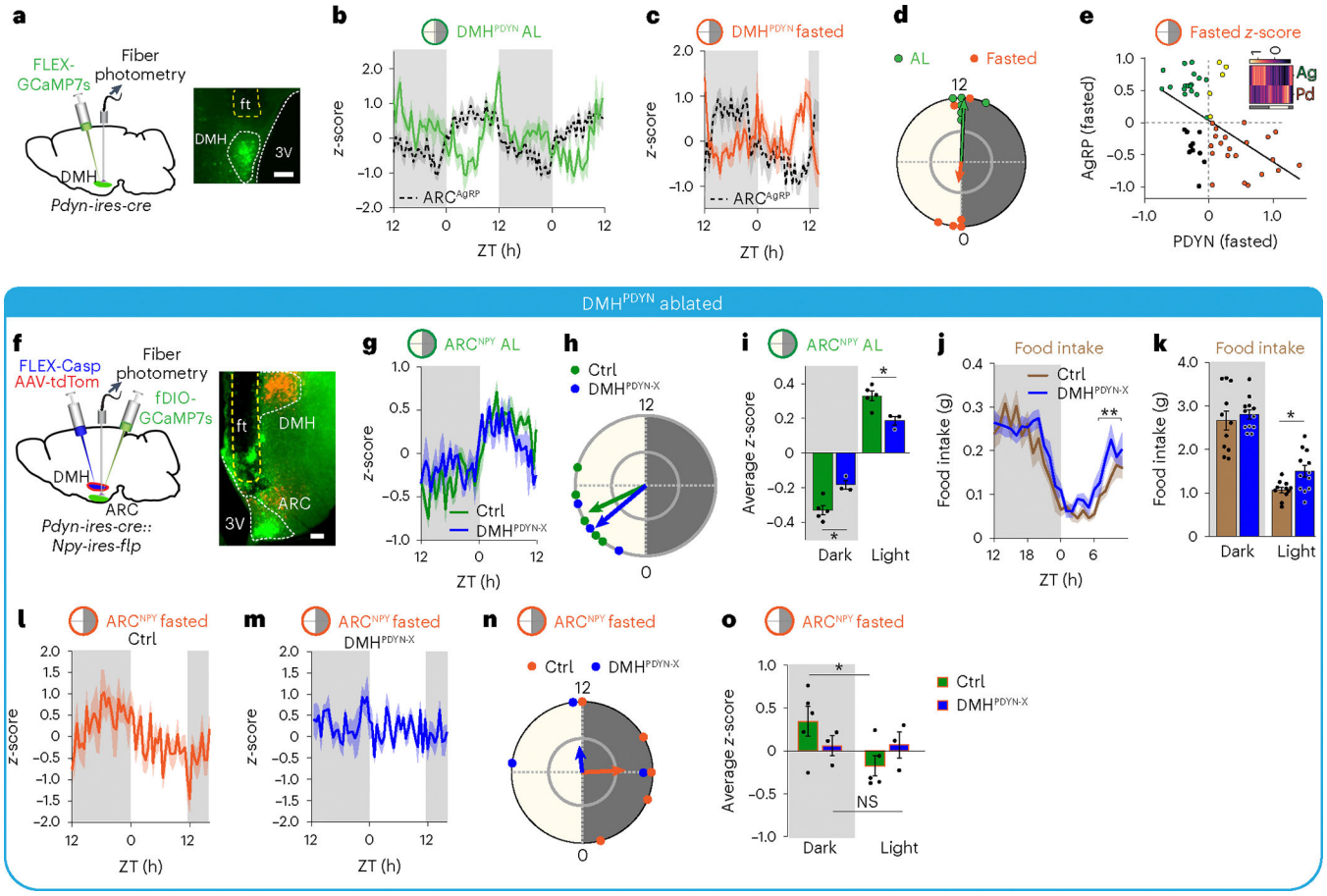

Fig. 4 |. Impairing input from DMH^{PDYN} neurons attenuates free-feeding AgRP activity rhythms.

a, Schematic and representative image of in vivo fiber photometry recording of PDYN neuron Ca^{2+} activity in DMH. Scale bar, 300 μm. **b**,**c**, Average DMH^{PDYN} Ca^{2+} activity overlaid with AgRP-neuron activity (from Fig. 1) in AL (**b**) and fasted (**c**) states ($n = 6$ mice). **d**, Rayleigh plot of DMH^{PDYN} activity in AL fed (mean peak: ZT12.16, Rayleigh $P = 0.00048$) and fasted (mean peak time: ZT0.50, Rayleigh $P = 0.5499$) mice. Phases differ significantly ($P = 0.0070$, circular one-way ANOVA). **e**, Inverse correlation between average fasted DMH^{PDYN} and average AgRP activities ($r = -0.525$, $P < 0.0001$, two-tailed Pearson correlation). Inset: heat map of average AgRP and DMH^{PDYN} activity in fasted animals. Ag, AgRP; Pd, DMH^{PDYN}. **f**, Schematic of in vivo fiber photometry recording from ARC^{NPY} neurons in mice with DMH^{PDYN} ablation (DMH$^{PDYN\text{-}X}$). Representative images of ARC:GCaMP7s and DMH showing AAV-tdTomato marking the site of caspase injection (upper left). Scale bar, 200 μm. **g**, Average ARC^{NPY} GCaMP activity in DMH$^{PDYN\text{-}X}$ or intact DMH^{PDYN} neurons (Ctrl). Average of 8 d from three mice. **h**, Rayleigh plot of ARC^{NPY} GCaMP activity in DMH$^{PDYN\text{-}X}$ mice (mean peak: ZT3.34, Rayleigh $P = 0.06$) versus Ctrl (mean peak: ZT4.37, Rayleigh $P = 0.0082$). Phases do not differ significantly. **i**, Comparison of average dark and light phase ARC^{NPY} activity in mice with or without DMH^{PDYN} ablation (two-sided, unpaired *t*-test, $P = 0.0118$ for light and $P = 0.0134$ for dark phase, $n = 5$ Ctrl and $n = 3$ DMH$^{PDYN\text{-}X}$ mice). **j**,**k**, Feeding pattern of DMH$^{PDYN\text{-}X}$

mice (**j**, ** $P = 0.00998$) and total consumed food during daytime and nighttime (**k**, * $P = 0.00104$) compared to control animals (two-tailed, unpaired *t*-test, $n = 11$ Ctrl and $n = 12$ $DMH^{PDYN\text{-}X}$ mice). **l**,**m**, Average ARC^{NPY} Ca^{2+} activity in fasted condition in Ctrl (**l**) and $DMH^{PDYN\text{-}X}$ (**m**) mice ($n = 5$ (**l**) and $n = 3$ (**m**)). **n**, Rayleigh plot of ARC^{NPY} GCaMP activity in fasted Ctrl (mean peak: ZT17.81, not significant) and $DMH^{PDYN\text{-}X}$ (mean peak: ZT11.59, not significant) mice. Phases do not differ significantly. **o**, Comparison of average dark time and light time ARC^{NPY} GCaMP activity in Ctrl and $DMH^{PDYN\text{-}X}$ mice in fasted state (two-sided, unpaired *t*-test, * $P = 0.0231$, $n = 6$ Ctrl and $n = 3$ $DMH^{PDYN\text{-}X}$ mice). Data are presented as mean ± s.e.m. For exact *P* values and statistics, see Fig. 4 Source Data. Ctrl, control; ft, fiber tract; 3V, third ventricle; NS, not significant.

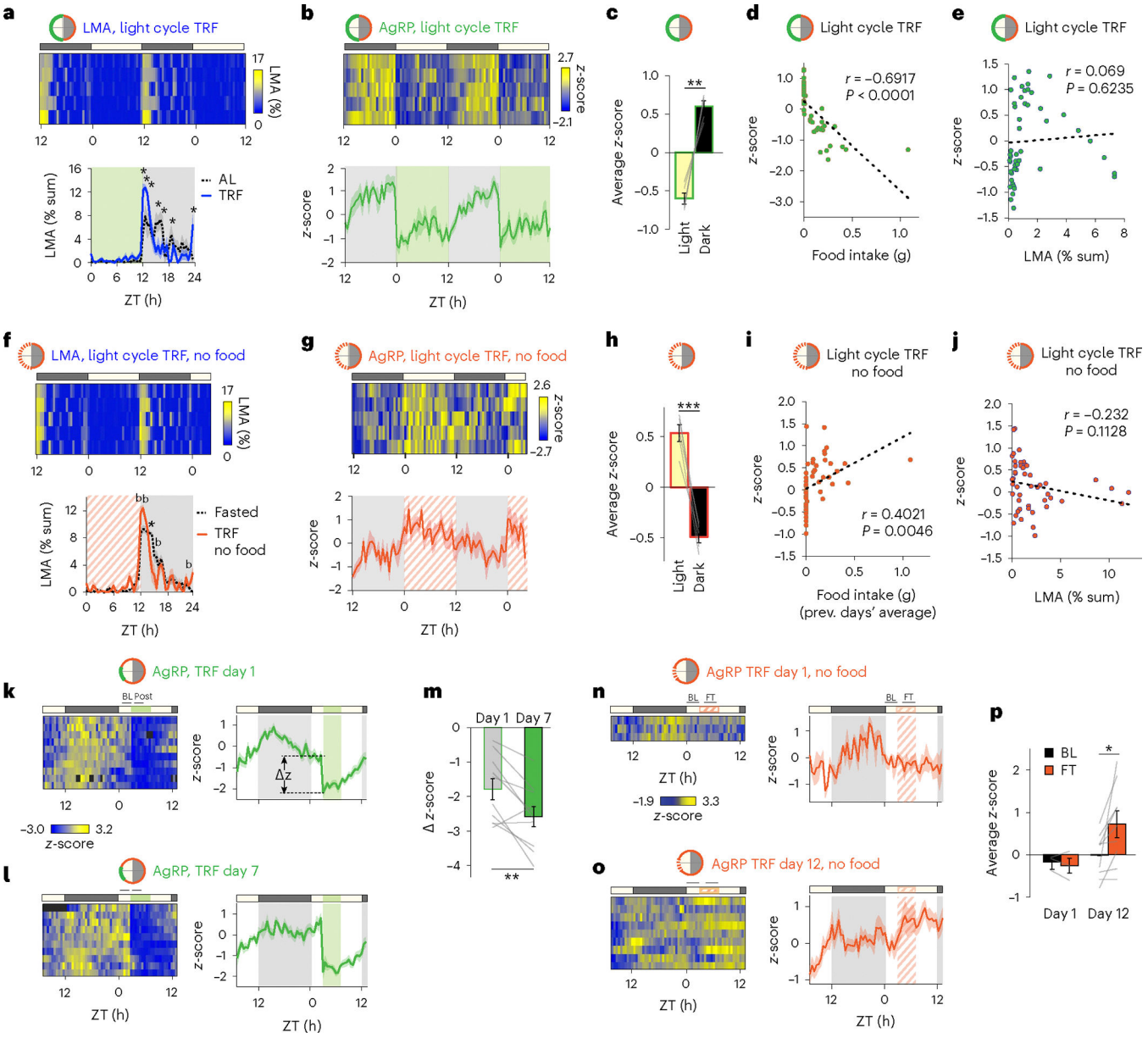

Fig. 5 |. Time-restricted food availability prevails photic cues in determining AgRP-neuron activity rhythms.

a,**b**, Locomotor activity (LMA) (**a**) and AgRP GCaMP7s activity (**b**) of animals subjected to light phase TRF (food available between ZT0 and ZT12). Upper panels: heat maps showing individual recordings; lower panels: averaged activities ($n = 5$ mice, $^{*}P < 0.05$, two-tailed paired *t*-test). Green shade and rims show food availability. Orange rims show absence of food. Dashed black line (**a**): LMA of the same animals under AL conditions. **c**, Average AgRP-neuron activity during light and dark phases ($P = 0.0012$, two-tailed paired *t*-test, $n = 5$ mice). **d**,**e**, Two-tailed Pearson correlation of AgRP activity levels with food intake (**d**) and LMA (**e**) across the same circadian timepoints. **f**–**j**, Same with **a**–**e** but under fasted conditions ($^{*}P = 0.0143$, $^{b}P < 0.01$, $^{***}P = 0.0002$, two-tailed paired *t*-test, $n = 5$). Orange striped shade and rims show food availability in previous days. **k**,**l**, AgRP-neuron activity in

mice subjected to TRF between ZT3-ZT7 on day 1 (**k**) and day 7 (**l**) shown as individual (left, heat maps) and averaged (right panels) data. **m**, Change in *z*-score (*z*-score at ZT2.5 (before food is available) − *z*-score at ZT3 (food provided)) in TRF days 1 and 7 ($P = 0.0087$, two-tailed paired *t*-test, $n = 10$ mice). **n**,**o**, Same as **k**,**l** but under fasted conditions and day 12 instead of day 7. FT, food access time in the previous days. **p**, Average *z*-score before (ZT0–ZT3) and during (ZT4–ZT7) entrained feeding window without food (day 12, $P = 0.022$, two-tailed paired *t*-test, $n = 3$ mice on day 1 and $n = 9$ mice on day 12). Data are presented as mean ± s.e.m. For exact *P* values and statistics, see Fig. 5 Source Data. prev., previous.

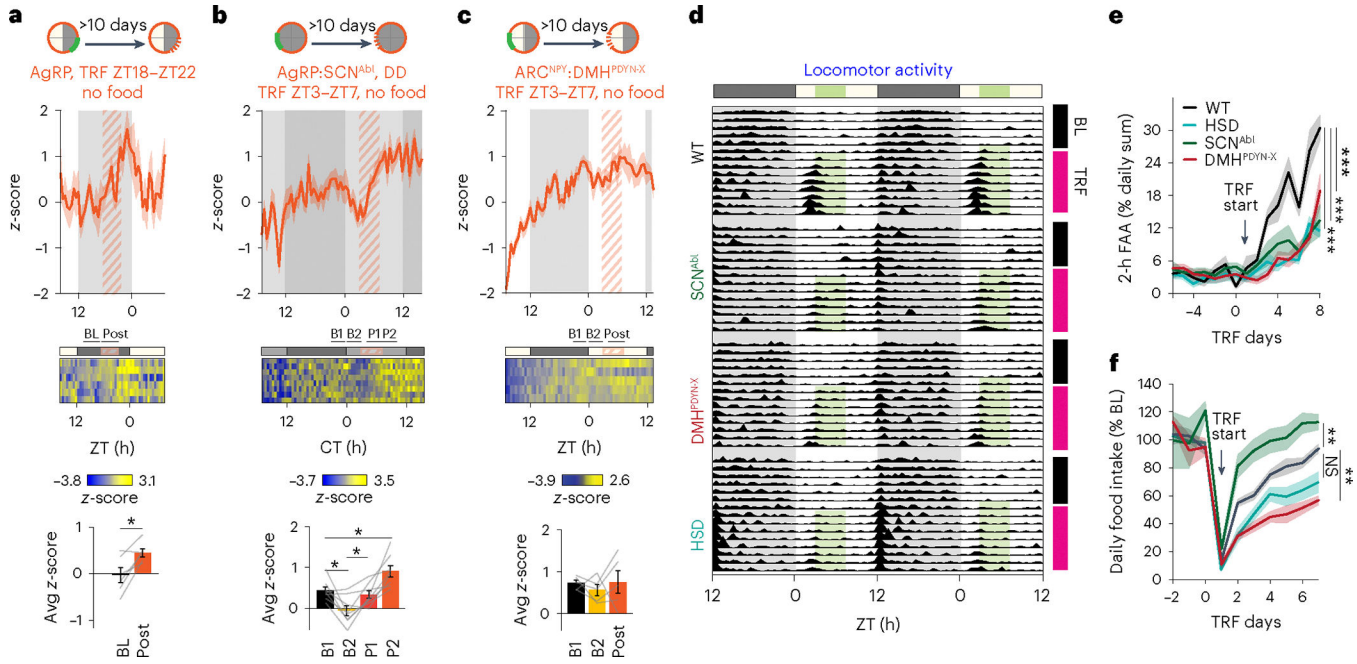

Fig. 6 |. Ablating DMH^{PDYN} neurons impairs AgRP-neuronal and behavioral adaptation to TRF.

a, AgRP-neuron activity recorded from mice that had been subjected to TRF between ZT18 and ZT22 for 17 d and were provided no food during the recording period. Orange shades depict food access periods during TRF days. Upper panel: average of $n = 6$ animals; middle panel: individual data from each animal; lower panel: comparison of AgRP activity in baseline (BL) (ZT14–ZT17.5) and post-food time (ZT18–ZT22) periods (*$P = 0.0174$, two-tailed paired *t*-test). **b**,**c**, AgRP-neuron and ARC$^{NPY/AgRP}$-neuron activities recorded under DD conditions (**b**, *$P < 0.0469$) and from DMH^{PDYN}-ablated mice (**c**), respectively. Mice had been subjected to TRF between ZT3 and ZT7 for more than 10 d and were provided no food during the recording period. Upper panels: average of $n = 8$ mice (**b**) and $n = 5$ mice (**c**); middle panels: individual data from each animal; lower panels: comparison of AgRP/NPY activity in BL-1 (before light phase, ZT21–ZT0), BL-2 (light onset, before food, ZT0–ZT3) and post-food time (Post or P1, ZT4–ZT7) or P2 (ZT7–ZT10, **b**) periods. One-way ANOVA followed by Tukey's multiple comparison test. **d**, Double actogram showing locomotor activity in wild-type (WT), SCN^{Abl}, DMH^{PDYN}-ablated and AgRP-specific 11βHSD2-expressing mice in BL (AL, black vertical lines) and TRF days (pink vertical lines, green shade marking the food availability during TRF days). **e**,**f**, Two-hour food-anticipatory activity (one-way ANOVA of area under the curve ($F_{3,21} = 22.03$, $P < 0.0001$), with Dunnet's correction for multiple comparisons (**e**)) and daily food intake (as percent of average of BL days, one-way ANOVA of area under the curve ($F_{3,21} = 19.99$, $P < 0.0001$), followed by Dunnet's correction for multiple comparisons (**f**)) in control, SCN^{Abl}, DMH^{PDYN-X} and HSD mice. *$P < 0.05$, **$P < 0.01$ and ***$P < 0.0001$. TRF starts on day 1. Data are presented as mean ± s.e.m. For exact *P* values and statistics, see Fig. 6 Source Data. Avg, average; NS, not significant.

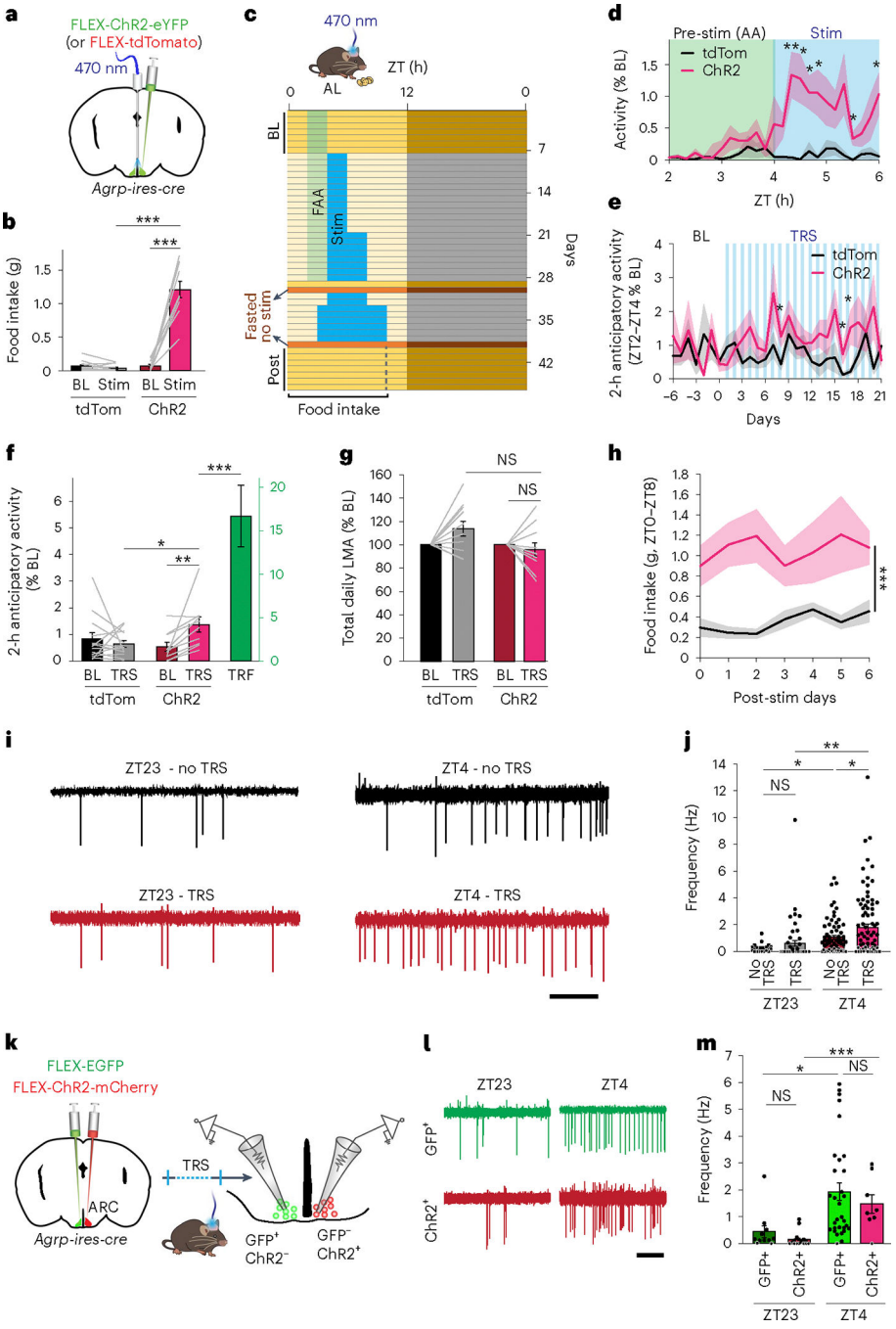

Fig. 7 |. Rhythmic AgRP stimulation partially mimics food entrainment.

a, Schematic of in vivo optogenetic stimulation of AgRP neurons. **b**, Confirmation of successful AgRP stimulation with increased 2-h food intake in ChR2-transduced mice compared to tdTomato-transduced control (Ctrl) mice ($n = 12$ Ctrl and $n = 10$ ChR2 mice, two-tailed paired and unpaired t-tests, ***$P < 0.0001$). **c**, Schematic for AgRP optoentrainment protocol by time-restricted stimulation (TRS). **d**, Locomotor activity from a representative day (day 7) of TRS, shown as a percentage of average baseline (BL) activity, focusing on the FAA (green) and optostimulation (blue) periods ($n = 12$ Ctrl mice and n

= 10 ChR2 mice, two-tailed, unpaired *t*-test, **P* < 0.05 and ***P* < 0.01). **e**, Comparison of 2-h FAA in ChR2 and Ctrl mice during BL and 21 d of TRS (*n* = 11–13 Ctrl mice and *n* = 10 ChR2 mice, two-tailed unpaired *t*-test, **P* < 0.05). **f**, Average 2-h FAA (average of TRS day 3 to day 21) in ChR2 and tdTomato mice (*n* = 13 Ctrl and *n* = 10 Chr2 mice, two-way ANOVA with Sidak's correction, **P* = 0.023 and ***P* = 0.0046), in comparison to 2-h FAA from mice going through TRF (day 9, *n* = 10 mice, two-tailed unpaired *t*-test, ****P* = 0.00042). **g**, Average of total daily locomotor activity on BL days in comparison to TRS days (days 3–21, *n* = 11 Ctrl mice and *n* = 10 ChR2 mice, two-tailed paired and unpaired *t*-tests). **h**, Evaluation of first 8 h of light-phase food intake after 29 d of TRS, in AL mice, without any stimulation (*n* = 10 Ctrl mice and *n* = 4 ChR2 mice, two-tailed unpaired *t*-test, ****P* < 0.0001). **i**,**j**, Representative loose-seal traces from mice culled after 2 weeks of optoentrainment (**i**; scale bar, 2 s) and average firing rate (**j**, *n* = 17–71 neurons from Ctrl mice and 50–89 neurons from ChR2 mice, two-tailed unpaired *t*-test, **P* < 0.03 and ***P* = 0.00250). **k**, Schematic showing delivery of GFP-expressing and ChR2-expressing virus on contralateral sides of the ARC and subsequent optoentrainment. **l**, Representative traces of loose-seal recordings showing spontaneous AgRP-neuron activity from mice undergoing optoentrainment. Scale bar, 2 s. **m**, Average firing rate of $GFP^{+}ChR2^{-}$ and $GFP^{-}ChR2^{+}$ AgRP neurons from the contralateral sides of the same acutely prepared ARC slice (*n* = 11–31 GFP neurons and *n* = 12–15 ChR2 neurons, two-sided unpaired *t*-test, **P* = 0.0132 and ****P* = 0.0000836). Data are presented as mean ± s.e.m. For exact *P* values, number of subjects/neurons and statistics, see Fig. 7 Source Data. NS, not significant.